Article

Cancer Cell

A Platform of Synthetic Lethal Gene Interaction Networks Reveals that the *GNAQ* Uveal Melanoma Oncogene Controls the Hippo Pathway through FAK

Graphical Abstract

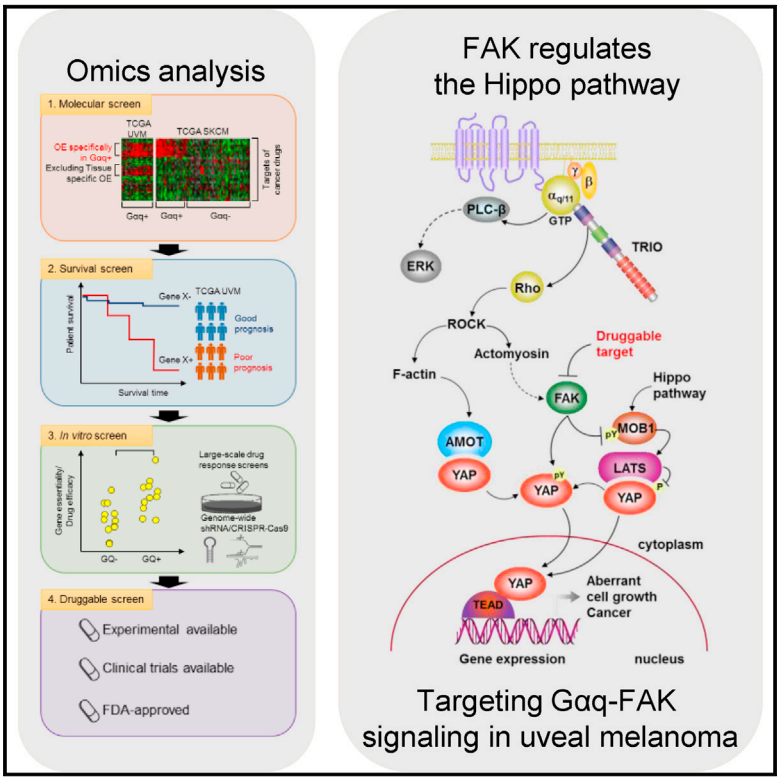

Highlights

- Innovative bioinformatics pipeline reveals FAK as candidate synthetic lethal with Gαq
- FAK is a central mediator of the *GNAQ*-driven oncogenic signaling circuitry
- FAK activates YAP by MOB1 phosphorylation resulting in Hippo pathway inhibition
- FAK represents a potential precision therapeutic target for uveal melanoma treatment

Authors

Xiaodong Feng, Nadia Arang, Damiano Cosimo Rigiracciolo, ..., Qianming Chen, Eytan Ruppin, J. Silvio Gutkind

Correspondence

lee.joosang@gmail.com (J.S.L.), qmchen@scu.edu.cn (Q.C.), eyruppin@gmail.com (E.R.), sgutkind@ucsd.edu (J.S.G.)

In Brief

Using a bioinformatics analysis, Feng et al. identify FAK as a vulnerability of uveal melanoma (UM) with oncogenic Gαq and show that inhibition of FAK reduces UM growth. Gαq activates FAK via the non-canonical TRIO-RhoA pathway, and FAK in turn regulates YAP, known to be critical for UM, by phosphorylating MOB1.

Feng et al., 2019, Cancer Cell *35*, 1–16
March 18, 2019
https://doi.org/10.1016/j.ccell.2019.01.009

CellPress

Please cite this article in press as: Feng et al., A Platform of Synthetic Lethal Gene Interaction Networks Reveals that the *GNAQ* Uveal Melanoma Oncogene Controls the Hippo Pathway through FAK, Cancer Cell (2019), https://doi.org/10.1016/j.ccell.2019.01.009

Cancer Cell
Article

A Platform of Synthetic Lethal Gene Interaction Networks Reveals that the *GNAQ* Uveal Melanoma Oncogene Controls the Hippo Pathway through FAK

Xiaodong Feng,[1,2,10] Nadia Arang,[1,3,10] Damiano Cosimo Rigiracciolo,[1,7] Joo Sang Lee,[4,8,11,*] Huwate Yeerna,[1] Zhiyong Wang,[1,3] Simone Lubrano,[1] Ayush Kishore,[1] Jonathan A. Pachter,[6] Gabriele M. König,[5] Marcello Maggiolini,[7] Evi Kostenis,[5] David D. Schlaepfer,[1] Pablo Tamayo,[1,9] Qianming Chen,[2,11,*] Eytan Ruppin,[4,8,11,*] and J. Silvio Gutkind[1,11,12,*]

[1]Moores Cancer Center, University of California, San Diego, La Jolla, CA 92093, USA
[2]State Key Laboratory of Oral Diseases, National Clinical Research Center for Oral Diseases, West China Hospital of Stomatology, Sichuan University, Chengdu 610041, China
[3]Biomedical Sciences Graduate Program, University of California, San Diego, La Jolla, CA 92093, USA
[4]Cancer Data Science Laboratory, National Cancer Institute, National Institute of Health, Bethesda, MD 20892, USA
[5]Molecular, Cellular and Pharmacobiology Section, Institute of Pharmaceutical Biology, University of Bonn, Bonn 53115, Germany
[6]Verastem Oncology, Needham, MA, USA
[7]Department of Pharmacy and Health and Nutritional Sciences, University of Calabria, Rende 87036, Italy
[8]Center for Bioinformatics and Computational Biology & Department of Computer Sciences, University of Maryland, College Park, MD 20742, USA
[9]Division of Medical Genetics, UC San Diego School of Medicine, La Jolla, CA 92093, USA
[10]These authors contributed equally
[11]Senior author
[12]Lead Contact
*Correspondence: lee.joosang@gmail.com (J.S.L.), qmchen@scu.edu.cn (Q.C.), eyruppin@gmail.com (E.R.), sgutkind@ucsd.edu (J.S.G.)
https://doi.org/10.1016/j.ccell.2019.01.009

SUMMARY

Activating mutations in *GNAQ/GNA11*, encoding Gαq G proteins, are initiating oncogenic events in uveal melanoma (UM). However, there are no effective therapies for UM. Using an integrated bioinformatics pipeline, we found that *PTK2*, encoding focal adhesion kinase (FAK), represents a candidate synthetic lethal gene with *GNAQ* activation. We show that Gαq activates FAK through TRIO-RhoA non-canonical Gαq-signaling, and genetic ablation or pharmacological inhibition of FAK inhibits UM growth. Analysis of the FAK-regulated transcriptome demonstrated that *GNAQ* stimulates YAP through FAK. Dissection of the underlying mechanism revealed that FAK regulates YAP by tyrosine phosphorylation of MOB1, inhibiting core Hippo signaling. Our findings establish FAK as a potential therapeutic target for UM and other Gαq-driven pathophysiologies that involve unrestrained YAP function.

INTRODUCTION

Recent advances in omics technologies have enabled the sequencing and characterization of cancers to an unprecedented depth, revealing mechanisms of growth and molecular drivers of disease. Bioinformatics analyses of these data have demonstrated a large heterogeneity in genetic drivers, highlighting complex biological networks toward the identification of therapeutic targets. These large-scale genomics efforts have revealed a small set of cancers that are driven by only a

Significance

Despite the central role of Hippo/YAP-regulating mechanisms in uveal melanoma (UM), there are no clinically effective therapeutic targets. Dissection of mediators regulating Hippo/YAP signaling could identify urgently needed therapeutic opportunities to inhibit YAP-dependent tumor growth in UM and other cancers. Coupling the power of an unbiased computational pipeline to the unique genetic landscape of UM, we uncovered a molecular framework regulating YAP and identified FAK as a druggable signaling hub downstream of *GNAQ* in UM. Gαq activates tyrosine phosphorylation networks through FAK, which activates YAP by a mechanism suppressing the Hippo kinase cascade. FAK inhibitors suppress YAP activation *in vivo* and halt UM growth, exposing a signaling vulnerability that can be targeted for UM treatment.

A

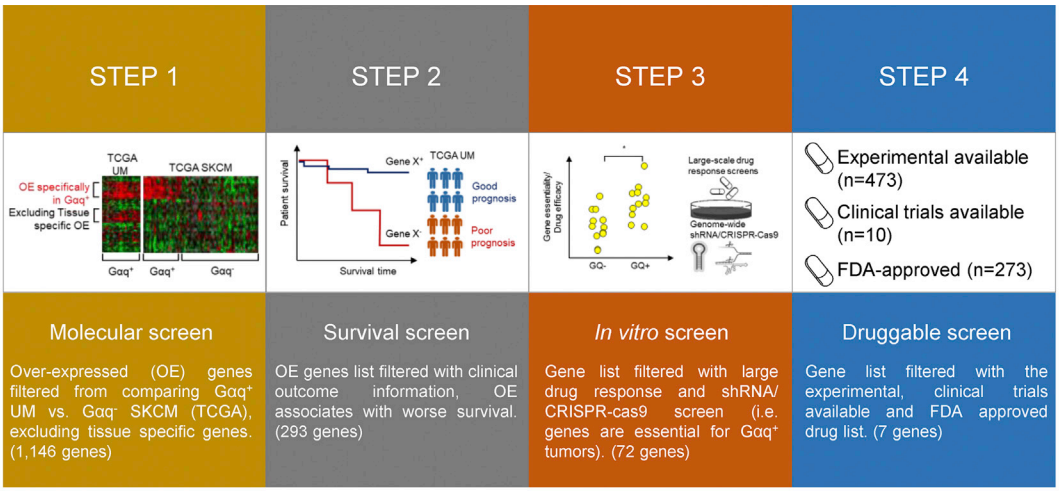

B

Genes	Molecular	Clinical	Phenotypic	SL-score	Viability %
PTK2	1.05E-09	1.71E-03	8.62E-03	0.94	40.35
MGLL	6.62E-04	1.87E-02	6.01E-03	0.78	75.57
AKT1	8.71E-03	1.29E-02	2.21E-02	0.64	39.16
SIRT1	6.20E-04	9.29E-02	3.55E-02	0.53	66.38
MTHFD1	4.42E-02	4.43E-03	3.50E-02	0.50	61.64
CDK1	8.14E-03	9.20E-03	7.12E-02	0.50	35.99
PSMB5	3.93E-02	9.97E-04	4.36E-01	0.36	64.76
GNAQ					26.06

C

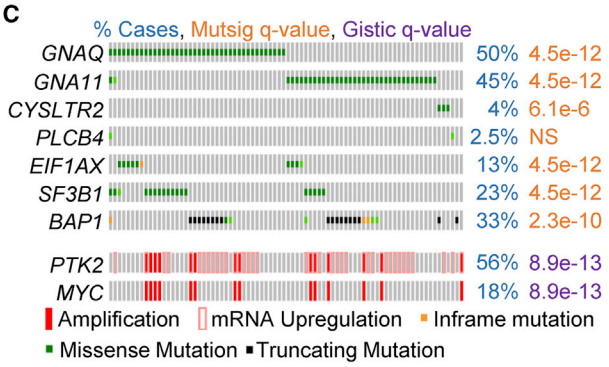

D

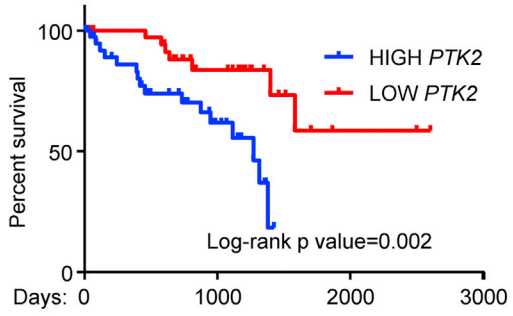

E

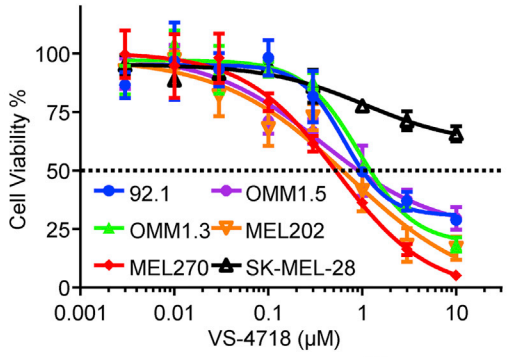

F

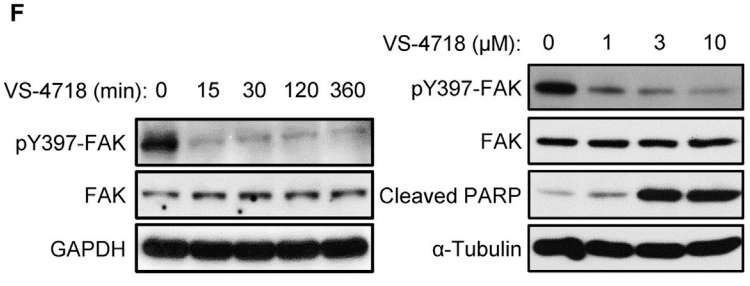

G

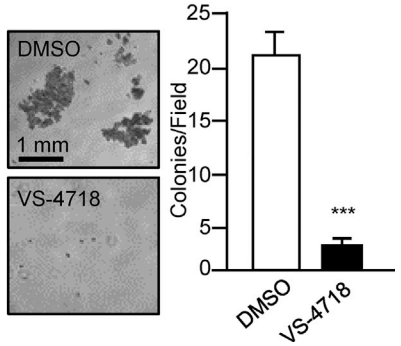

(legend on next page)

select number of mutational events. One such cancer, uveal melanoma (UM), is characterized by a gain-of-function mutation in the heterotrimeric G protein, Gαq. A hotspot mutation in *GNAQ* or in *GNA11* results in encoding constitutively active Gαq proteins rendering them as driver oncogenes in approximately 93% of UM (Van Raamsdonk et al., 2009, 2010). Another ~4% of UM harbor activating mutations in *CYSLTR2*, a Gαq-linked G protein-coupled receptor (GPCR) (Moore et al., 2016), firmly establishing UM as a Gαq-driven malignancy.

Aberrant activity of G proteins and GPCRs have been frequently associated with an oncogenic state and promotion of tumorigenesis (Dorsam and Gutkind, 2007; O'Hayre et al., 2013). However, the precise molecular mechanisms by which prolonged Gαq signaling controls cancer cell growth are still under investigation. We and others have previously shown that these mechanisms are in part due to unique signaling circuitries that lead to the activation of YAP, a transcriptional co-activator regulated by the Hippo pathway. In turn, YAP activation is necessary for UM growth (Feng et al., 2014b; Yu et al., 2014a). As a key downstream target of the tumor suppressive Hippo signaling cascade, YAP is over-activated in multiple cancers (Moroishi et al., 2015; Yu et al., 2015). Despite this, pharmacological targeting of YAP or the Hippo pathway has been challenging. Verteporfin, an ophthalmological drug, inhibits YAP-TEAD interaction, which is the major transcriptional factor regulated by YAP, in UM (Feng et al., 2014b; Yu et al., 2014a) with some anecdotal clinical success (Barbazetto et al., 2003; Soucek and Cihelkova, 2006). However, the potential for verteporfin as a therapeutic has been hindered by its high systemic toxicities after prolonged use (Arnold et al., 2004; Azab et al., 2004). Currently, no effective therapeutic targets are available for UM, and no specific YAP inhibitors are currently in clinical use (Moroishi et al., 2015). A more complete understanding of Hippo/YAP-regulating mechanisms in cancer could identify urgently needed therapeutic opportunities to inhibit YAP-dependent tumors, including UM.

The highly distinctive and well-defined genetic landscape of UM provides a unique opportunity for the application of unbiased bioinformatics approaches to investigate the precise molecular mechanisms by which prolonged Gαq signaling controls cancer cell growth, and how these pathways can be targeted for precision therapies of Gαq-driven pathophysiologies.

RESULTS

A Bioinformatics Pipeline Identifies *PTK2* as a Druggable Candidate Synthetic Lethal Gene with *GNAQ*

To identify the specific vulnerabilities of *GNAQ*-driven tumors, we adapted our recently established bioinformatics pipeline that identifies clinically relevant synthetic lethal interactions (termed ISLE) (Lee et al., 2018). We denote a sample with mutations in or amplification of *GNAQ*, *GNA11*, or *CYSLTR2* as Gαq$^+$, and a sample without any of these genetic alterations as Gαq$^-$. Adapting the rationale of the ISLE pipeline to our aim here, a candidate gene was determined to be a synthetic lethal (and thus a druggable vulnerability) of Gαq$^+$ tumors if it satisfies the following four conditions (Figure 1A): (1) molecular condition: Gαq$^+$ tumor should differentially overexpress the candidate gene versus Gαq$^-$ samples, (2) clinical condition: overexpression of the candidate gene should be associated with poor survival of patients with Gαq$^+$ tumors, (3) phenotypic condition: the candidate gene is significantly more essential in Gαq$^+$ than in Gαq$^-$ cell lines, and (4) druggable condition: targeting the candidate gene products with inhibitors is significantly more effective in Gαq$^+$ than in Gαq$^-$ cell lines, i.e., Gαq$^+$ cell lines are more sensitive to cell growth inhibition by the candidate inhibitors than Gαq$^-$ cell lines.

Our analysis therefore proceeded along four steps. First, taking advantage of the publicly available TCGA (The Cancer Genome Atlas) (Cancer Genome Atlas Research Network et al., 2013) data, we extracted genes that are differentially overexpressed in Gαq$^+$ UM (>96%). Since there are insufficient UM Gαq$^-$ samples, we used Gαq$^-$ skin cutaneous melanoma (SKCM) samples as a control. Indeed, we observed significant overlap in the overexpressed genes in Gαq$^+$ UM and Gαq$^+$ SKCM samples (hypergeometric $p < 4.83 \times 10^{-199}$, see the STAR Methods) compared with Gαq$^-$ SKCM samples, justifying the use of Gαq$^-$ SKCM samples as a control for Gαq$^+$ UM. We excluded genes overexpressed in UM compared with SKCM irrespective of Gαq status to control for cancer type-specific differential expression. Second, among the genes that pass the first filter, we identified those whose expression correlates with poor prognosis of UM patients. Third, we further selected those genes from *in vitro* functional screens that show significantly higher essentiality (or drug response) in Gαq$^+$ cancer cell lines following

Figure 1. Bioinformatics Analysis Reveals FAK as Critical for UM Progression

(A) Pipeline to discover druggable therapeutic targets in UM: molecular screen, survival screen, *in vitro* screen, and druggable screen.

(B) Summary of the final seven gene hits. Molecular, clinical, phenotypic, and synthetic lethal (SL) scores were calculated as in Lee et al. (2018). Cell viability was assessed *in vitro* in UM cells (OMM1.3) following siRNA-mediated inhibition of each gene (cell viability normalized to OMM1.3 treated with non-targeting siRNA, siRNA-*GNAQ* used as positive control, mean, n = 3).

(C) Oncoprint depicting the genomic landscape of TCGA UM cohort (Robertson et al., 2017) downloaded from cBioPortal (Gao et al., 2013). Each bar represents one sample and their respective gene mutation or expression status. Percentage of gene alterations (in blue) and MutSig (in orange) or Gistic Q value (in purple) is listed on the right.

(D) Kaplan-Meier plot depicting overall survival for UM patients stratified against *PTK2* expression in their tumors. *PTK2*-high and *PTK2*-low groups are defined as top and bottom 50% of *PTK2* expression. p = 0.002.

(E) UM cell lines (Mel270, 92.1, OMM1.3, OMM1.5, and MEL202 with *GNAQ* active mutation) cell viability assay after treatment with 1 μM FAK inhibitor (VS-4718), SKCM cells (SK-MEL-28) served as control. Data are the percent viability normalized to vehicle treatment (mean ± SEM, n = 3).

(F) Immunoblot of OMM1.3 cells showing pY397-FAK after treatment with VS-4718 (1 μM) (left) and cleaved PARP in response to 36 h VS-4718 (1–10 μM) treatment (right).

(G) Representative images (left) and quantification (right) of colony formation assay of OMM1.3 cells with VS-4718 treatment in semisolid media (mean ± SEM, n = 3; ***p < 0.001, DMSO treatment as control); scale bar, 1 mm.

See also Figure S1.

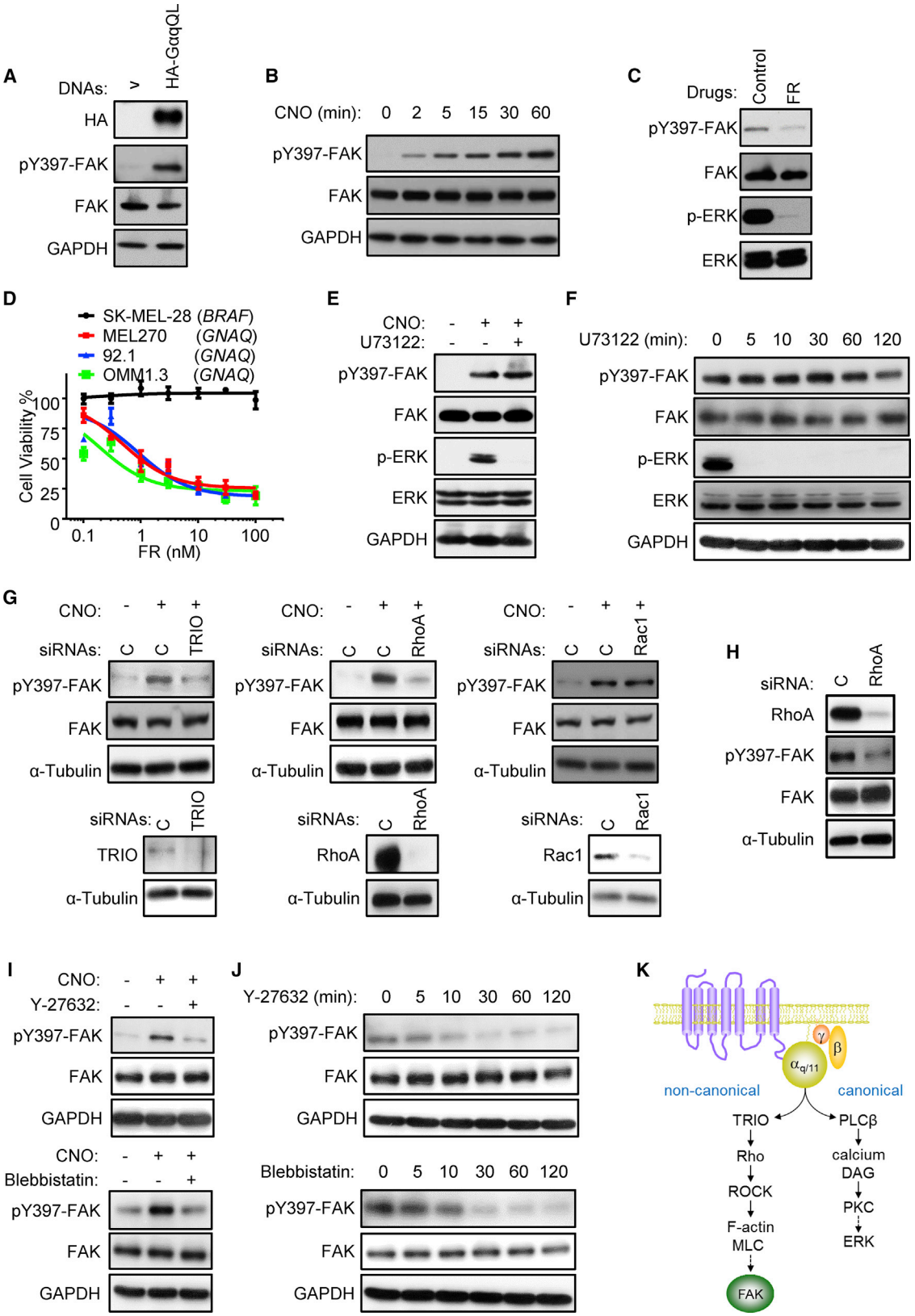

(legend on next page)

the standard procedure to determine cancer cell dependency (Tsherniak et al., 2017). Lastly, we selected only those genes that are druggable, i.e., targets of known cancer drugs (Figure 1A). We performed cell viability assays after small interfering RNA (siRNA)-mediated gene inhibition, confirming the vulnerabilities of our predicted hits in Gαq$^+$ cells (Figure 1B). This four-step Gαq$^+$ synthetic lethal (SL) identification process results in seven predicted SL genes, which play roles in multiple biological processes, including cell growth, cell survival, lipid metabolism regulation, cell-cycle control, and the processing of class I MHC peptide, all of which reduced cell growth when knocked down. Among them, the top predicted gene, *PTK2*, encoding focal adhesion kinase (FAK), reduced cell viability almost 60% after inhibition using *PTK2*-specific siRNA knockdown (Figure 1B).

PTK2 is not mutated in UM, a disease that is characterized by mutations, primarily mutually exclusive activating mutations in *GNAQ*, *GNA11*, and *CYSLTR2*, and mutually exclusive mutations in genes encoding two RNA splicing factors, *EIF1AX* and *SF3B1*, or a deubiquitinase *BAP1*, as depicted in (Figure 1C) (Moore et al., 2016; Robertson et al., 2017; Van Raamsdonk et al., 2009, 2010). Instead, statistically significant gain of chromosome 8q (Robertson et al., 2017), including *PTK2* and *MYC*, occurs in UM. Interestingly, *PTK2* and *MYC* are amplified in 18% of UM cases (TCGA), and 38% of UM cases also exhibit *PTK2* mRNA upregulation independent of amplification (Figure 1C). In total, 56% of UM cases have *PTK2* gene amplification or mRNA upregulation (Figure 1C). Interestingly, we found that expression of *PTK2* is significantly correlated with reduced overall patient survival (Figure 1D). Strikingly, a pan-cancer analysis of alteration frequency of *PTK2* reveals that UM has the highest alteration frequency among all available TCGA solid tumor cohorts (Figure S1A). We next tested the sensitivity of five representative UM cell lines, 92.1, OMM1.3, OMM1.5, Mel270, and Mel202, all of which harbor *GNAQ* mutations, to FAK inhibition using VS-4718, an orally bioavailable FAK inhibitor (FAKi) (Sulzmaier et al., 2014), using the SKCM cell line SK-MEK-28 (*BRAF* mutant) as a control. *In vitro*, UM cell lines demonstrate a dose-dependent sensitivity to FAK inhibition with a half maximal effective concentration (EC_{50}) of around 1 μM (Figure 1E). Similar results were obtained with PF562771, a chemically distinct FAKi (Figure S1B). Instead, the SK-MEK-28 cell line was largely insensitive to FAKi, with an EC_{50} > 10 μM for VS-4718 (Figure 1E). siRNA knockdown of FAK reduced cell viability in two representative UM cells nearly as potently as Gαq (encoded by *GNAQ*) knockdown (Figures S1C–S1F). Gαq knockdown reduced the accumulation of FAK in its active, tyrosine 397-phosphorylated form (pY397-FAK) (Sulzmaier et al., 2014) (Figure S1D), while FAK knockdown reduced total FAK and pY397-FAK protein levels, as expected (Figure S1E). FAKi inhibited FAK rapidly (Figures S1F and S1G), and resulted in UM apoptosis as judged by the accumulation of cleaved PARP (Figure 1F). We further assessed whether inhibition of FAK impacted the oncogenic potential of UM cells by measuring their clonogenic capacity in semisolid medium and found that FAKi nearly abolished the colony formation ability of UM cells (Figure 1G). Together, these findings support that FAK may be required for *GNAQ*-driven UM cell proliferation, survival, and clonogenic growth, thereby representing a potential therapeutic target for the treatment of UM.

The Canonical Gαq Signaling Pathway Is Dispensable but a TRIO-RhoA Non-canonical Signaling Mechanism Is Evident for FAK Activation

We next sought to investigate the mechanism by which Gαq controls FAK. To understand the impact of *GNAQ* mutation on FAK activation, we express a hemagglutinin (HA)-tagged activated Gαq mutant, Gαq-Q209L (HA-GαqQL), observed in UM and an empty vector control in HEK293 cells. Immunoblotting against total and phosphorylated forms of FAK revealed that phosphorylation of FAK at Y397 was significantly increased after expression of GαqQL (Figure 2A). We next took advantage of a previously established synthetic Gαq-coupled GPCR (Gαq-DREADD) that can be activated by a synthetic ligand, clozapine N-oxide (CNO) (Armbruster et al., 2007; Vaque et al., 2013). We stimulated Gαq-DREADD-expressing HEK293 cells with CNO over a time course and found increasingly elevated levels of pY397 FAK in response to CNO (Figure 2B). In UM cells, Gαq knockdown by siRNA or inhibition by FR900359 (FR), a potent Gαq inhibitor (Schrage et al., 2015), diminished FAK and extracellular signal-regulated kinase (ERK) activation (Figures 2C and S1D). Consistent with these data, Gαq inhibition with FR in UM cells and SKCM cells showed inhibition of cell proliferation only in UM cells (Figure 2D). These results support the notion that FAK acts downstream of the Gαq in UM. However, it is

Figure 2. Gαq Regulates FAK Activation through a Non-canonical TRIO/RhoA-Mediated Signaling Circuitry

(A) Immunoblot depicting phosphorylation of FAK after transfection with HA-GαqQL and control expression vectors in HEK293 cells.

(B) Immunoblot showing FAK phosphorylation in Gαq-DREADD-expressing HEK293 cells stimulated with CNO (1 μM) over a time course analysis.

(C) Immunoblot depicting FAK and ERK phosphorylation after 2 h FR (1 μM) treatment in OMM1.3 cells.

(D) UM cell viability assay after 72 h treatment with FR, SK-MEL-28 *BRAF* SKCM served as control, percent viability is normalized to vehicle treatment (mean ± SEM, n = 3).

(E) Immunoblot showing phosphorylation of ERK and FAK after stimulation of Gαq-DREADD-expressing HEK293 cells with CNO (1 μM) at 5 min in combination with 1 h U73122 (1 μM) pre-treatment.

(F) Immunoblot showing phosphorylation of ERK and FAK during a time course of treatment with GF109203X (1 μM) in OMM1.3 cells.

(G) Immunoblot showing FAK phosphorylation in Gαq-DREADD-expressing HEK293 cells after 5 min of CNO stimulation (1 μM) in combination with siRNA-mediated TRIO, RhoA, or Rac1 knockdown (top), and immunoblot to show efficiency of siRNA-mediated TRIO, RhoA, or Rac1 knockdown (bottom).

(H) Immunoblot showing FAK phosphorylation after siRNA-mediated RhoA knockdown in OMM1.3 cells.

(I) Immunoblot showing FAK phosphorylation in Gαq-DREADD-expressing HEK293 cells after 5 min of CNO stimulation (1 μM) in combination with 1 h Y-27632 (10 μM) pre-treatment (top), and in combination with 1 h blebbistatin (20 μM) pre-treatment (bottom).

(J) Immunoblot showing FAK phosphorylation during a time course of treatment with Y-27632 (top) and blebbistatin (bottom) in OMM1.3 cells.

(K) Cartoon depicting the non-canonical signaling pathway regulating FAK activation by Gαq. G protein βγ subunits are depicted in addition to Gαq. DAG, diacylglycerol; MLC, myosin light chain.

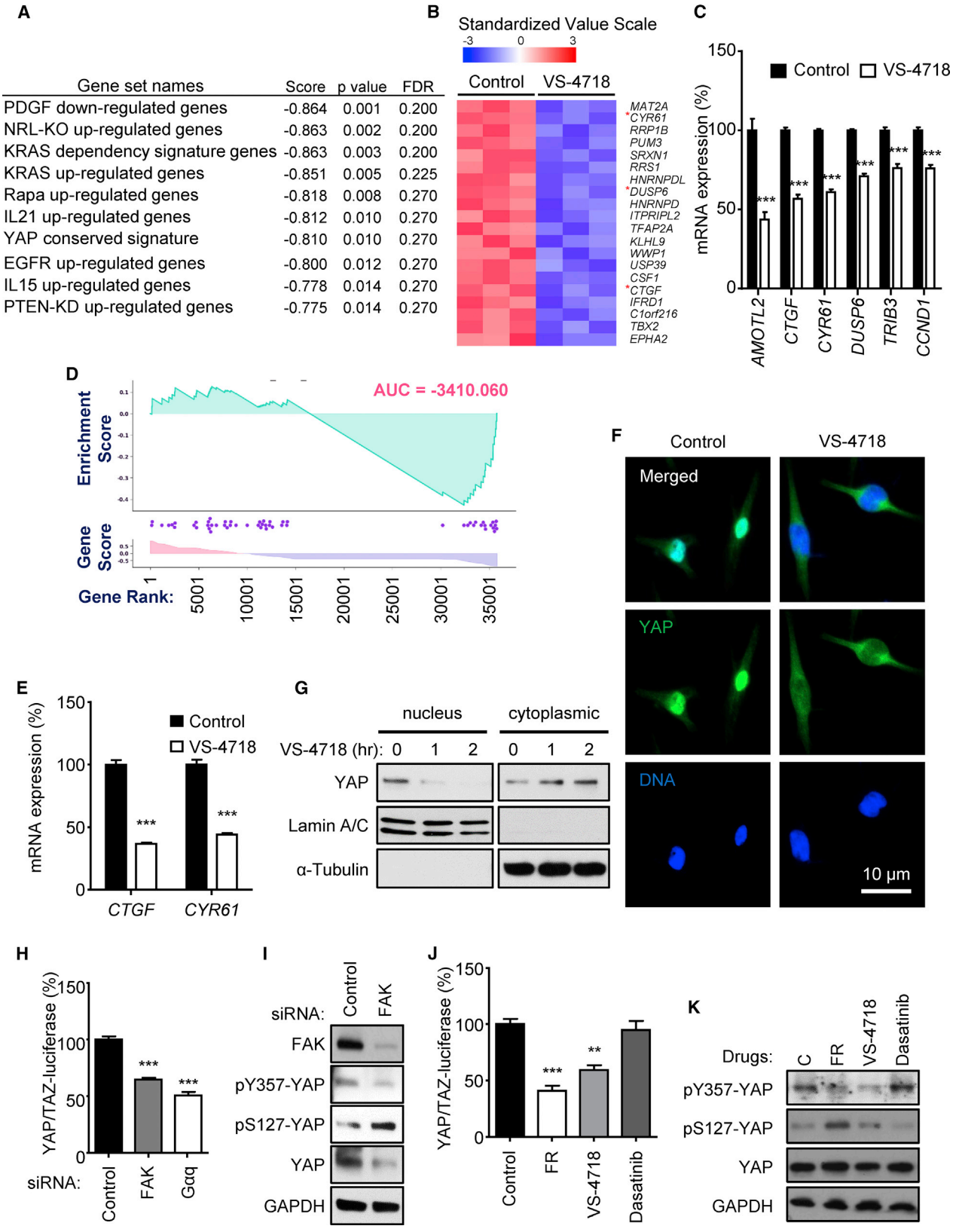

(legend on next page)

unclear which of the multiple Gαq or Gαq-coupled receptor-initiated signaling pathways are responsible for regulating FAK activation.

Phospholipase Cβ (PLCβ)-dependent second messenger activation is among the best-known downstream events stimulated by Gαq (Griner and Kazanietz, 2007; Hubbard and Hepler, 2006), and is considered to be the canonical Gαq signaling pathway, causing transient ERK activation (Vaque et al., 2013). Inhibition of PLCβ by the use of a small-molecule PLC inhibitor (U73122) abolished the ERK activation, as we reported previously (Vaque et al., 2013), but did not have an impact on the activation of FAK (Figure 2E). Similarly, inhibition of protein kinase C (PKC) blocked ERK activation but not FAK in UM cells (Figure 2F), indicating that FAK may be activated independently of PLCβ. As Gαq activation of the AP1 and YAP transcriptional programs involves the stimulation of the TRIO guanine nucleotide exchange factor (GEF) for Rho GTPases (Feng et al., 2014b; Vaque et al., 2013), we next asked if this non-canonical Gαq signaling pathway is involved in FAK activation by Gαq. Knockdown of TRIO or RhoA prevented the activation of FAK by Gαq-DREADD in HEK293 cells and Gαq in UM cells (Figures 2G and 2H). In line with these findings, knockdown of Rac1 had no impact on FAK activation (Figure 2G). Further analysis showed that blocking actin polymerization by inhibiting ROCK or actomyosin contraction by Y-27632 (Ikeda et al., 2003; Narumiya et al., 2000) and blebbistatin (Kovacs et al., 2004), respectively, repressed FAK activation by Gαq-DREADD in HEK293 cells and Gαq in UM cells (Figures 2I and 2J). Together, these findings suggest that Gαq stimulates FAK independently of PLCβ and PKC, but instead through a non-canonical TRIO-dependent pathway resulting in RhoA activation and consequent cytoskeletal changes and actomyosin-initiated cell contraction and signaling (Figure 2K).

FAK Inhibition Represses the Transcriptional Activity of YAP

FAK is at the intersection of multiple signaling pathways that promote cancer progression (Sulzmaier et al., 2014), but it is not clear which downstream targets of FAK play a critical role in UM. As an approach to identify key downstream targets of the Gαq-FAK signaling axis, we performed transcriptomic RNA sequencing on UM cells treated with FAKi, and performed gene set enrichment analysis (Subramanian et al., 2005) to characterize the transcriptional effects of inhibiting Gαq and FAK at the pathway level using over 10,000 gene sets from the Molecular Signatures Database, including two sub-collections of oncogenic signatures and hallmark gene sets that we added to the database (Liberzon et al., 2015). Despite this large collection of transcriptional regulated genes, only 20 oncogenic signature gene sets were significantly repressed and 5 were activated by FAKi in UM cells (Figures 3A and S2A). These include the downregulation of genes described as stimulated by KRAS and epidermal growth factor receptor and cytokines such as interleukin-21 (IL-21) and IL-15, consistent with the likely role in the activation of growth-promoting pathways by FAK (Sulzmaier et al., 2014). FAKi also reduced the expression of genes repressed by JAK2, p53, and BMI, suggesting that FAK inhibition may trigger a p53-response and stimulate BMI and JAK2, all of which may contribute to FAK-dependent cell growth and warrant further investigation. One intriguing observation was that FAKi treatment resulted in a significant downregulation of YAP-signature genes (Zhao et al., 2008) (Figures 3A–3D, S2A, and S2B). The involvement of Hippo/YAP signaling in cancer progression as well as previous work demonstrating the key role of YAP signaling in UM (Feng et al., 2014b; Yu et al., 2014a, 2014b) led us to pursue this specific gene signature. To validate these findings, we performed qPCR for the classical YAP-target genes *CTGF* and *CYR61* in UM cells and found significant reduction in the presence of FAKi and knockdown of FAK or Gαq (Figures 3E, S2C, and S2D). We also found that FAKi clearly diminished YAP nuclear accumulation through quantification of anti-YAP staining and western blot analysis of nuclear and cytoplasmic cellular fractions (Figures 3F, 3G, and S2E). We further confirmed the functional impact of FAKi and FAK knockdown on YAP by performing YAP/TAZ luciferase reporter assays, and using Gαq inhibition and knockdown as a control (Figures 3H–3K, see Figures S1D and S1E for knockdown validation). Interestingly, inhibition of Gαq or FAK or siRNA-mediated FAK knockdown repressed YAP phosphorylation on tyrosine 357 (Y357) and increased phosphorylation on serine 127 (S127), which is one of the main repressive targets of Hippo signaling (Pan, 2010) (Figures 3I and 3K). We recapitulated these findings in heterologous systems, using HEK293 cells-expressing Gαq-DREADD stimulated with CNO and HEK293 cells expressing GαqQL. In both cases, FAK inhibition or knockdown reduced YAP pY357 and increased

Figure 3. FAK Inhibition Regulates the Hippo-YAP Pathway in UM

(A) The top 10 downregulated oncogenic signature gene sets of OMM1.3 cells treated with VS-4718 (1 μM, 2 h, vehicle treatment as control).

(B) Heatmap depicting the most downregulated genes by VS-4718 treatment as in (A), *YAP signature genes.

(C) mRNA expression level of YAP signature genes from RNA sequencing data (mean ± SEM, n = 3).

(D) Enrichment plot for YAP conserved signature gene set (GSEA, http://software.broadinstitute.org/gsea/index.jsp).

(E) mRNA expression of *CTGF* and *CYR61* measured by qPCR in OMM1.3 cells after 2 h VS-4718 treatment (1 μM, vehicle treatment as control, mean ± SEM, n = 3).

(F) Immunofluorescent staining of endogenous YAP (green) and Hoeschst staining for nuclear DNA (blue) in OMM1.3 cells after 4 h VS-4718 (1 μM) treatment, vehicle treatment as control; scale bar 10 μm.

(G) Immunoblot showing YAP nuclear and cytoplasmic localization after 2 h VS-4718 (1 μM) treatment in OMM1.3 cells, using lamin A/C and α-tubulin as nuclear and cytoplasmic markers, respectively.

(H) YAP/TAZ luciferase reporter assay after siRNA-mediated FAK and Gαq knockdown in OMM1.3 cells (mean ± SEM, n = 3).

(I) Immunoblot showing YAP phosphorylation after siRNA-mediated FAK knockdown in OMM1.3 cells.

(J) YAP/TAZ luciferase reporter assay after 2 h treatment with FR, VS-4718, or Dasatinib (all used at 1 μM) in OMM1.3 cells (mean ± SEM, n = 3).

(K) Immunoblot showing YAP phosphorylation after 2 h FR (1 μM), VS-4718 (1 μM), or Dasatinib (1 μM) treatment in OMM1.3 cells. In all cases $^{**}p < 0.01$; $^{***}p < 0.001$.

See also Figures S2 and S3.

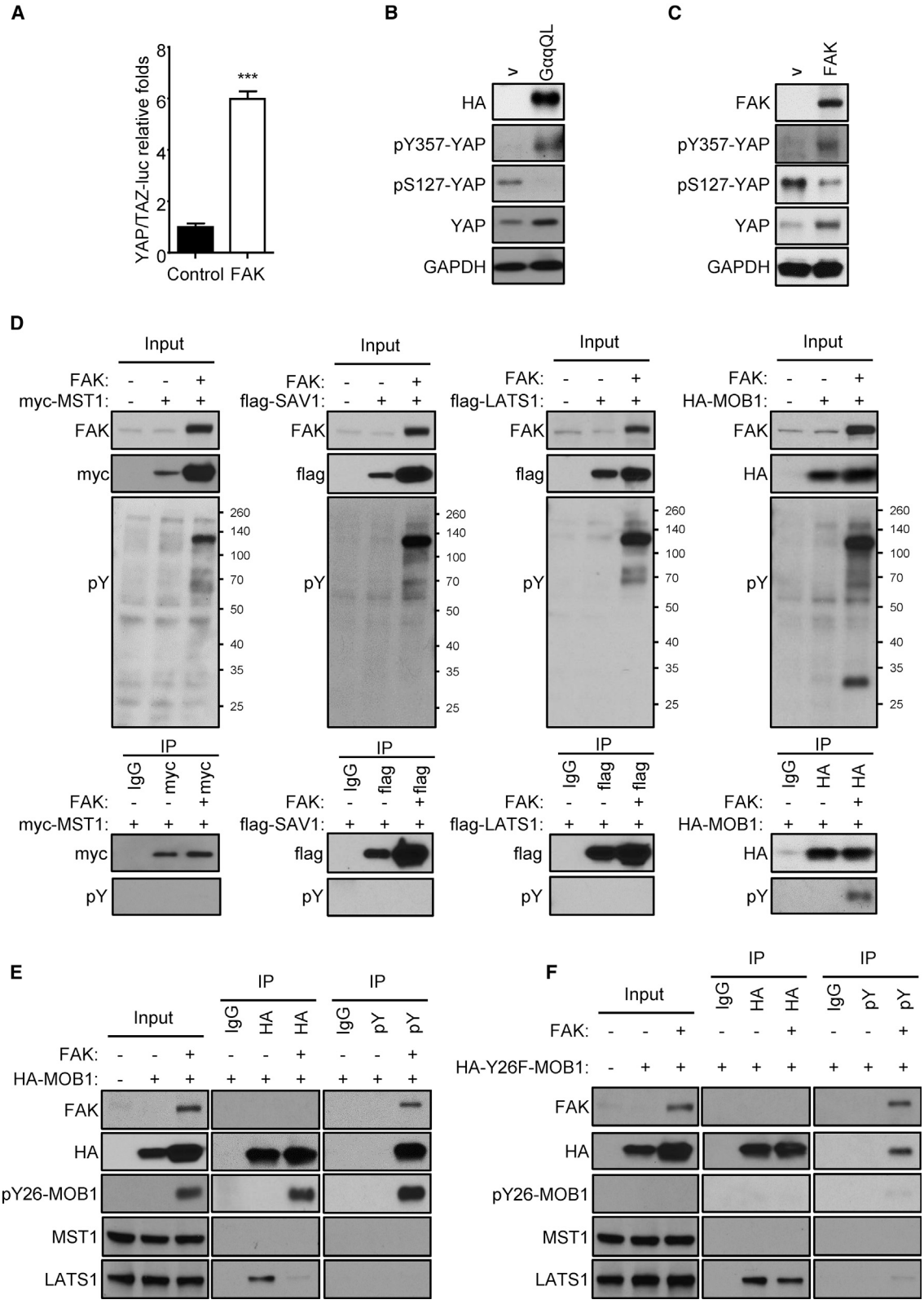

Figure 4. FAK Regulates YAP Activation through MOB-Y26 Phosphorylation, Disrupting the Core Hippo Kinase Signaling Pathway

(A) YAP/TAZ luciferase reporter assay after transient transfection of FAK and control expression vectors in HEK293 cells (mean ± SEM, n = 3; ***p < 0.001).

(B) Immunoblot showing phosphorylation status of YAP after transfection of HA-GαqQL and control expression vectors in HEK293 cells.

(legend continued on next page)

pS127, and reduced mRNA levels of YAP targets and YAP activity measured by luciferase reporter assay (Figures S3A–S3E), similar to UM cells. Inhibition of SRC in UM cells had no impact on YAP activity, measured by YAP/TAZ luciferase reporter assay, and failed to promote changes in YAP phosphorylation status (Figures 3J and 3K). Together, these results suggest that Gαq and FAK regulate YAP activation in UM, and that this process is likely independent of SRC.

FAK Regulates YAP Activation through YAP Tyrosine Phosphorylation and Inhibition of Hippo Core Kinases

We sought to further investigate the impact of FAK on YAP activity and found that overexpression of FAK in HEK293 cells leads to a significant increase of YAP activity (Figure 4A). It is well established that YAP activity and stability is tightly controlled by its phosphorylation on a number of residues (Moroishi et al., 2015; Yu et al., 2015). To define the phosphorylation state of YAP in the context of aberrant Gαq signaling, we expressed GαqQL and active FAK in HEK293 cells. Overexpression of GαqQL or FAK led to increased YAP protein level, diminished YAP pS127, and increased YAP pY357 (Figures 4B and 4C).

Regarding the changes in YAP pS127 levels, we hypothesized that FAK may also repress inhibitory signals to YAP from the Hippo pathway through direct phosphorylation on the core kinases of the Hippo pathway. In the canonical Hippo pathway, MST1/2 kinases bound to their regulatory protein SAV1 to activate the LATS1/2 kinases (collectively referred to as LATS) as part of a complex with MOB1A/B. LATS in turn phosphorylates YAP (or in certain cells TAZ) at multiple serine residues, including S127, leading to YAP inactivation by cytoplasmic retention and subsequent degradation (Moroishi et al., 2015; Pan, 2010; Yu et al., 2015). By a systematic analysis of the tyrosine phosphorylation status of each Hippo core kinase cascade component after co-transfection with FAK, we found only MOB1A to be tyrosine phosphorylated, as judged by its detection with anti-phosphotyrosine antibodies in tagged MOB1A immune precipitates (Figure 4D). MOB1 plays a critical regulatory role in the Hippo signaling cascade by transferring the upstream signal from the kinase complex of MST1/SAV1 to LATS (Meng et al., 2016). Consistent with our findings, scanning through large phosphoprotein databases (PhosphoSitePlus PTM Resource), we found that Y26 on MOB1A/B is conserved among mammals, and that this particular residue is phosphorylated in numerous high-throughput phosphoproteomic datasets (n = 161) (Figure S4A). To interrogate the functional impact of this phosphorylation on MOB1, we transfected HEK293 cells with HA-MOB1 and performed anti-HA and anti-pY immunoprecipitation assays. We found that an anti-pY26 MOB1 antibody recognized MOB1 only when co-transfected with FAK, which was abolished upon mutation of Y26 on MOB1 to Y26F (Figures 4E and 4F), thus serving as a specificity control. We further verified that FAK was able to directly phosphorylate MOB1 on its Y26 by *in vitro* kinase reaction using purified recombinant proteins (Figure S4B). When exploring the consequences of this post-translational modification in the assembly of Hippo kinase complexes, we found that phosphorylation on Y26-MOB1 by FAK dissociates the MOB1/LATS complex (Figure 4E). Strikingly, mutation of Y26 of MOB1 to Y26F rescued FAK-induced dissociation from LATS1 (Figure 4F) and abolished YAP activation by FAK (Figure S4C). Together, these data suggest that FAK regulates MOB1 Y26 phosphorylation, resulting in the dissociation of the functional MOB1/LATS complex, preventing Hippo-dependent inhibition of YAP and thereby promoting YAP activity.

FAK Inhibition Results in Increased MOB1/LATS Association and Signaling and Reduced YAP Protein Stability in UM

To study the effect of FAK inhibition on the Hippo pathway in UM cells, we examined the phosphorylation status of key Hippo pathway components after being treated with FAKi. We observed an increase of pS127-YAP, p909-LATS1, p1079-LATS1, a dose-dependent decrease in pY26 MOB1, and, in line with our previous data, enhanced MOB1/LATS interaction (Figures 5A, 5B, and S5A). In contrast, the MOB1-Y26F mutant demonstrated constitutively strong interaction with LATS independent of FAKi treatment (Figures S5B and S5C). Expression of MOB1-Y26F in UM cells phenocopied FAKi treatment as it diminished cell proliferation that could not be further reduced by FAKi (Figure S5D). Of interest, however, we did not observe an increase in p-MST1 in response to FAK inhibition (Figure 5A), nor a change in phosphorylation of MOB1 at T35, the main target of MST1 on MOB1 (Meng et al., 2016) with FAKi or knockdown of FAK (Figures S5B and S5C). This suggests that in UM, FAK regulates the link between LATS1 and YAP through MOB1, acting downstream of MST1 rather than controlling MST1 (Hippo) activity. In conjunction, we found FAK was able to phosphorylate YAP at Y357 *in vitro* (Figure S5E), a post-translational modification that has been shown to regulate YAP stability and activity (Li et al., 2016; Taniguchi et al., 2015), and, aligned with this finding, that FAK inhibition also caused diminished phosphorylation of Y357-YAP in UM cells (Figure 5A). Indeed, we confirmed that long-term (up to 36 h) FAK inhibition caused YAP protein down-regulation (Figure 5C). Furthermore, LATS1/2 knockdown was sufficient to rescue from the growth inhibition by FAKi in UM cells (Figure 5D), supporting that YAP signaling plays a key role in growth promotion downstream of FAK in UM cells. Altogether, our data suggest that FAK drives UM cell growth through promotion of YAP activity by coordinating the previously described

(C) Immunoblot showing phosphorylation status of YAP after transfection of FAK and control expression vectors in HEK293 cells.

(D) Immunoblot against phosphotyrosine after immunoprecipitation (IP) of tagged Hippo signaling core components (myc-MST1, flag-SAV1, flag-LATS1, or HA-MOB1) transfected with or without FAK in HEK293 cells. Total cell lysates (input) and IP by the indicated antibodies are shown. Western blot for FAK and each of the epitope tags are also shown.

(E) Immunoblot showing phosphorylation of MOB1 and association with MST1 and LATS1 after HA or pY IP in HEK293 cells transfected with or without FAK and wild-type HA-MOB1.

(F) Immunoblot showing phosphorylation of MOB1 and association with MST1 and LATS1 after HA or pY IP in HEK293 cells transfected with or without FAK and mutant HA-Y26F-MOB1.

See also Figure S4.

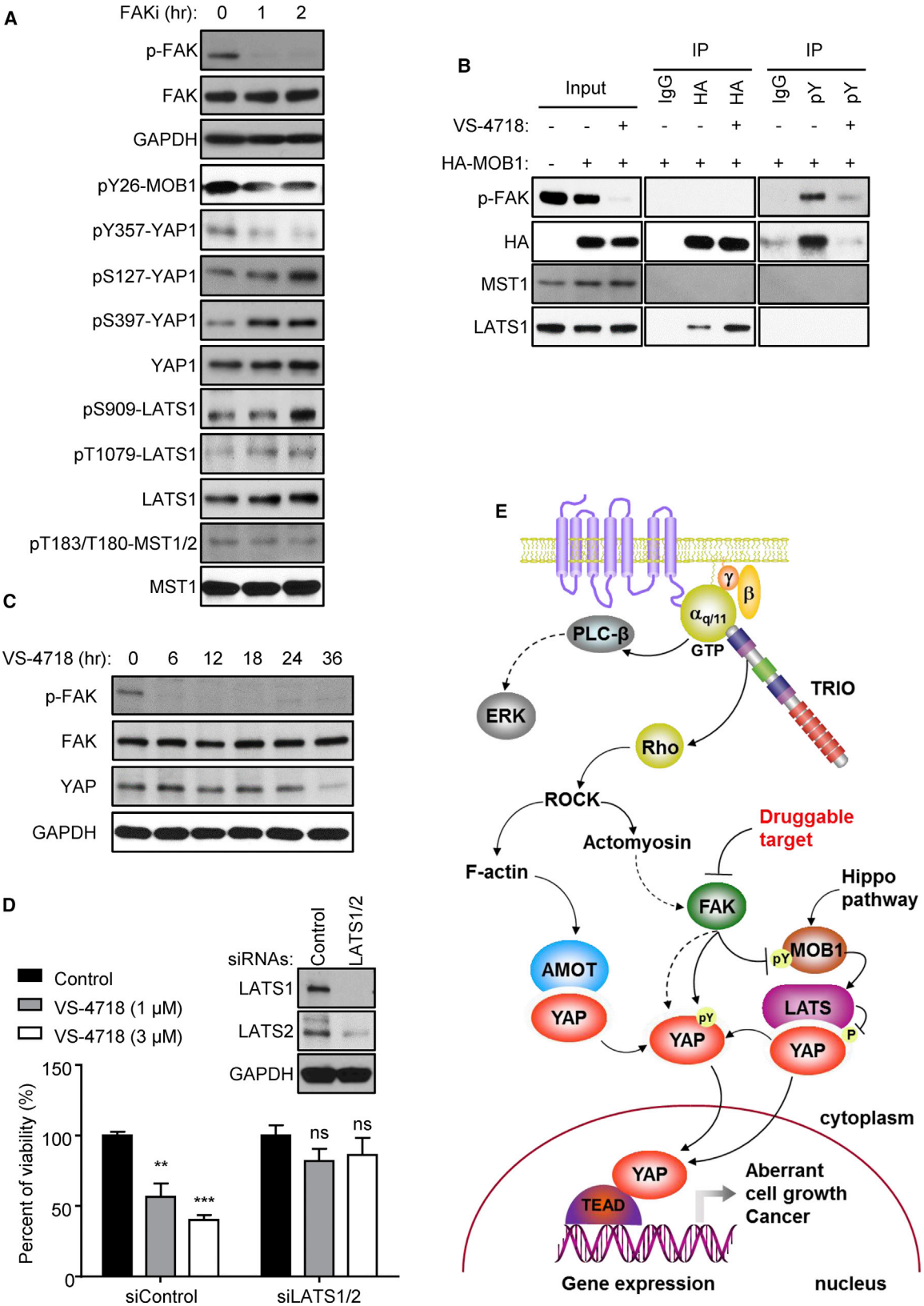

(legend on next page)

F-actin-mediated release of YAP from AMOT, which enhances the pool of cytosolic YAP and enables its nuclear translocation (Feng et al., 2014b), with the release of the inhibitory Hippo kinase cascade through the FAK-mediated phosphorylation of MOB1 and the concomitant tyrosine phosphorylation and stabilization of YAP (Figure 5E).

FAK Represents a Therapeutic Target in UM

We next tested the potential of FAK inhibition for UM treatment. For these studies, we first used lentiviral-delivered Cas9-sg*PTK2* to knockout (KO) *PTK2* in UM cells (Figure 6A). Most UM cells did not survive after genome editing of *PTK2* (not shown), only mass cultures of Mel270 targeted for *PTK2* grew in culture after puromycin selection, displaying nearly abolished FAK protein levels (Figure 6A). Re-expression of FAK under control of a doxycycline-inducible promoter was sufficient to rescue cell viability in UM cells in which FAK expression was reduced (Figure S6). We observed that *PTK2* KO cells developed only very small tumors (Figure 6B), suggesting that FAK activation is important for UM tumor growth *in vivo*. These observations further support the therapeutic potential of targeting FAK for UM. While there are multiple FAKi under clinical evaluation (Sulzmaier et al., 2014), VS-4718, chosen for our studies, was specifically designed for oral administration. We found that VS-4718 treatment reduces both UM tumor size and cell proliferation in two different UM tumor models (Figures 6C–6F). We observed clearly increased cytoplasmic retention of YAP in VS-4718-treated tumors, consistent with our previous findings that FAK controls YAP activity in UM cells (Figures 6G and 6H). These results suggest that the pharmacological inhibition of FAK may represent a viable therapeutic approach for the treatment of patients with UM harboring increased YAP activity.

DISCUSSION

The generation of massive quantities of genomic, epigenomic, and proteomic data has greatly enhanced our understanding of oncogenesis and cancer as a cellular state. The development of bioinformatics pipelines to predict nodes of connectivity between transcriptional and signaling networks can expedite efforts to identify and exploit molecular vulnerabilities for the treatment of cancer. We thus hypothesized that focusing on a cancer type specifically driven by few activating (Gαq) mutations may serve as a good testbed for studying such an approach, harnessing an SL-based integrated bioinformatics analysis to uncover potential oncogenic signaling mechanisms controlled by Gαq and target them. In this study, we demonstrate that FAK acts as a critical oncogenic signaling node in UM—mediating Gαq-driven regulation of the Hippo/YAP pathway and enabling the promotion of an oncogenic state. We provide evidence that FAK destabilizes interactions between key core Hippo pathway members thereby activating YAP in an MST1 (Hippo)-independent manner. Furthermore, we show that the oncogenic activity of FAK in UM is targetable by clinically relevant therapeutic agents.

The transformative potential of Gαq signaling was established in the early 1990s (Gutkind et al., 1991; Kalinec et al., 1992); however, the precise signaling events by which Gαq and its linked receptors transduce sustained proliferative signals is not yet well defined. This is due in part to the large number of second-messenger generating systems and signaling events that can be perturbed upon Gαq activation. The activation of these second-messenger systems and their direct targets, including ion channels and kinases such as PKC, calcium/calmodulin-dependent protein kinases, and mitogen-activated protein kinase (MAPK), are responsible for most of the rapid physiological responses elicited by GPCRs (Griner and Kazanietz, 2007; Howe, 2011; Julius and Nathans, 2012; Newton, 2010; Prevarskaya et al., 2011; Rozengurt, 2007; Sassone-Corsi, 2012). Recent studies have identified additional members of this network for UM, highlighting the role of GEFs such as RasGRP3 in MAPK activation (Chen et al., 2017). Despite this link, therapeutic strategies targeting MAPKs have yet to be successful. Clinical trials demonstrated that MEK inhibition with selumetinib or trametinib, as single agents or in combination with dacarbazine, has little impact on the overall survival of UM patients (Carvajal et al., 2014, 2018). This suggests that, although MEK/MAPK networks activated by PLCβ may contribute to UM initiation, they may not be critical for the maintenance of tumorigenic potential in UM.

Contrary to the transient nature of signal transmission through PLCβ, genome-wide RNAi screens revealed that the signaling events driven by Gαq that result in aberrant cell proliferation depends on highly specific protein-protein interactions, rather than solely on diffusible second messenger systems. Specifically, prior systems biology approaches have identified the RhoGEF TRIO as critical for activating Gαq-driven AP-1-regulated transcriptional networks independently of PLCβ to achieve sustained stimulation of proliferative pathways (Vaque et al., 2013). Further work has shown that this pathway converges in the activation of YAP and that YAP activation is critical for the oncogenic potential of UM (Feng et al., 2014a, 2014b; Yu et al., 2014a). The Hippo/YAP cascade is a key growth-regulating pathway in normal cellular physiology (Bhatt et al., 2010; Moroishi et al., 2015; Yu et al., 2015). Unsurprisingly, dysregulation of the Hippo pathway is seen frequently in cancer; however,

Figure 5. Inhibition of FAK Causes YAP Inhibition in UM by Unleashing Hippo Pathway Signaling, and Inducing Inhibitory YAP Phosphorylation and Degradation

(A) Immunoblot of total and phosphorylated core Hippo pathway members in OMM1.3 cells after 1 μM VS-4718 treatment for 0, 1, and 2 h.

(B) Immunoblot showing the association of MOB1 with LATS1 after HA or pY immunoprecipitation of OMM1.3 cells transfected with HA-MOB1 with or without 1 h VS-4718 treatment.

(C) Immunoblot showing levels of total YAP over a time course of 1 μM VS-4718 treatment in OMM1.3 cells.

(D) Immunoblot showing levels of LATS1/2 after knockdown in OMM1.3 cells (top) and cell viability assay of OMM1.3 cells with LATS1/2 knockdown in combination with VS-4718 treatment (bottom, mean ± SEM, n = 3; $^{**}p < 0.01$, $^{***}p < 0.001$; ns, not significant).

(E) Cartoon depicting the signaling pathway by which FAK mediates YAP activation downstream of constitutively active Gαq mutant in UM. See text for details. See also Figure S5.

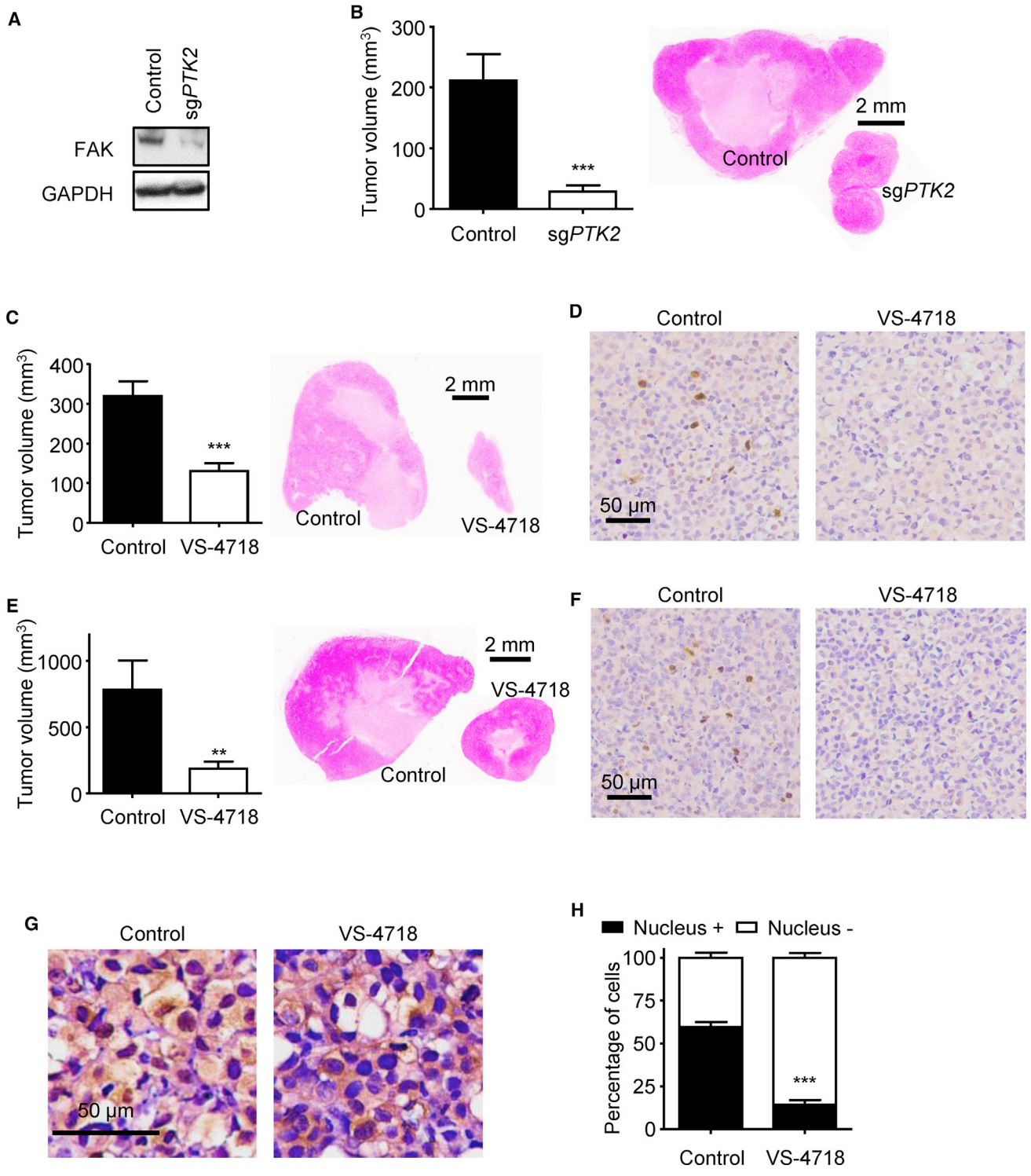

Figure 6. FAKi in UM Inhibits YAP-Dependent UM Tumor Growth

(A) Immunoblot showing CRISPR/Cas9-mediated *PTK2* knockout in Mel270 cells (wild-type as control).

(B) Tumor volume of *PTK2* knockout Mel270 cells *in vivo* (wild-type as control) at the end of the study (mean ± SEM, n = 4) (left) and H&E-stained sections of representative tumors from each group (right); scale bar, 2 mm.

(C) Tumor volume of Mel270 cells *in vivo* with or without VS-4718 treatment at the end of the study (mean ± SEM, n = 8) (left) and H&E-stained sections of representative tumors from each group (right), scale bar, 2 mm.

(D) Ki67 immunohistochemistry staining in Mel270 tumors with or without VS-4718 treatment; scale bar, 50 μm.

(legend continued on next page)

its core components are rarely mutated (Martin et al., 2018; Moroishi et al., 2015). Rather, external pressures from upstream oncogenes typically drive YAP-dependent cell proliferation. Identifying the key molecular players that facilitate oncogenic signaling through Hippo/YAP pathway may also uncover potential network vulnerabilities. Interestingly, inhibition of PLCβ does not impact the activation of YAP after Gαq stimulation (Feng et al., 2014b). Together, these findings suggest that the canonical Gαq-PLCβ-MAPK signaling axis may be critical for tumor initiation rather than tumor maintenance, and that opportunities for intervention may lie within the distinct signaling circuitry transduced through TRIO.

FAK is a non-receptor tyrosine kinase whose role as a downstream target of Gαq has been well established by biochemical studies (Gutkind and Robbins, 1992); however, the contribution of FAK as a mediator of oncogenic Gαq signaling has not been previously explored. Our finding that FAK is rapidly activated by Gαq-linked GPCRs and the oncogenic mutant Gαq through TRIO and RhoA, rather than PLCβ, prompted us to focus on the possibility that FAK may represent an integral component of the non-canonical pathway by which Gαq regulates aberrant cell growth. We found that inhibition of FAK was sufficient to reduce UM cell proliferation and, if prolonged, to trigger apoptotic cell death. This response was unanticipated as FAK inhibitors often have limited activity in most cancers as single agents but instead synergize with cytotoxic agents, as we have shown for ovarian cancer, which overexpresses FAK as a typical example (Sulzmaier et al., 2014). We hypothesized that, compared with other cancer types with FAK overexpression, the compounding impact of *PTK2* copy-number gain and overexpression together with Gαq-driven FAK activity in UM creates a unique cellular state that may be highly dependent on the activity of FAK and therefore highly sensitive to FAK inhibition. This convergence of computational predictions, and biochemical and genetic information, enabled the discovery of the therapeutic potential of inhibiting FAK for UM treatment.

FAK has been recently linked to YAP activity in mechanotransduction and in the coordination of cell proliferation and differentiation in mouse incisors during development (Hu et al., 2017; Lachowski et al., 2018). However, the underlying cell context-specific and developmental mechanisms are still not fully understood. We provide evidence that in UM the role of FAK converges on promoting YAP activity through the tandem inhibition of Hippo pathway signals by phosphorylation of Y26 of MOB1 and Y357 of YAP. In the case of YAP phosphorylation, these observations extend prior studies indicating the role of JAK2 and SRC in Y357 phosphorylation (Li et al., 2016; Taniguchi et al., 2015). However, downstream of FAK, we observed both tyrosine-phosphorylated YAP and a decrease in pS127 YAP, the latter a direct target of the Hippo signaling pathway. In this regard, there is increasing evidence suggesting that Hippo signaling is tightly regulated by the assembly and dissociation of key signaling complexes. Our interrogation of these complexes in response to FAK activation led to the finding that FAK phosphorylates MOB1 on Y26, resulting in the disassembly of the MOB1/LATS complex and disruption of the Hippo pathway downstream of MST1, effectively rewiring the molecular mechanisms controlling YAP activity. Mutation of Y26 of MOB1 is sufficient to abolish the effect of FAK. Whereas further work may be required to establish the structural basis for this inhibition, as well as alternative FAK-driven pathways in mechanotransduction and development, our findings support that disruption of the MOB1/LATS signaling complex by FAK is a key regulatory step resulting in YAP activation by Gαq. Ultimately, this mechanism may coordinate the Gαq-induced increase in cytosolic free YAP, which is mediated by Rho-induced actin polymerization (Feng et al., 2014b), with Hippo kinase cascade inhibition through the FAK-mediated phosphorylation of MOB1, resulting in the YAP-dependent UM cell growth.

The current lack of effective treatments for primary or metastatic UM leaves a large therapeutic gap for patients and clinicians underscoring an urgent need for the identification of additional pharmacological targets for therapeutic intervention. As YAP-targeting strategies have remained elusive thus far, the success of FAK inhibition in our *in vivo* models in the context of previously established success and safety of FAK inhibitors in human clinical trials highlights the translational potential of our findings and establishes FAK as a therapeutic target for the treatment of UM. Toward this end, the application of systems-level and bioinformatics investigation will be a powerful strategy to identify precision treatment options for UM and a myriad of Gαq-driven diseases.

STAR★METHODS

Detailed methods are provided in the online version of this paper and include the following:

- KEY RESOURCES TABLE
- CONTACT FOR REAGENT AND RESOURCE SHARING
- EXPERIMENTAL MODEL AND SUBJECT DETAILS
  - Human Tumors Xenografts and VS-4718 *In Vivo* Treatment
  - Cell Lines, Culture Procedures and Chemicals
  - DNA Constructs
- METHOD DETAILS
  - Bioinformatic Analysis (Identifying Clinically-Relevant Gαq-Specific Vulnerabilities of UM)
  - Immunoblot Assay
  - CRISPR-Cas9-Knockout
  - siRNAs Transfection
  - MOB1-Y26F Point Mutation
  - Immunofluorescence
  - Luciferase Assays

(E) Tumor volume of OMM1.3 cells *in vivo* with or without VS-4718 treatment at the end of the study (mean ± SEM, n = 4) (left) and H&E-stained sections of representative tumors from each group (right), scale bar, 2 mm.
(F) Ki67 immunohistochemistry staining of OMM1.3 tumors with or without VS-4718 treatment; scale bar, 50 μm .
(G) Representative YAP immunohistochemistry staining of Mel270 tumors with or without VS-4718 treatment; scale bar, 50 μm.
(H) Quantification of (G), showing fraction of cells with nuclear YAP localization (mean ± SEM, n = 3). In all cases ***p < 0.001.
See also Figure S6.

SUPPLEMENTAL INFORMATION

Supplemental Information includes six figures and can be found with this article online at https://doi.org/10.1016/j.ccell.2019.01.009.

ACKNOWLEDGMENTS

We thank Monica Acosta, James Nguyen, and Dana J. Steffen for their kind help and advice with some of the experiments. This work was supported by grants R33CA225291 (to J.S.G., J.S.L., and E.R.), U01CA217885 (to P.Y., J.S.G., and H.Y.), P30 CA023100 (to P.T. and H.Y.), R01HG009285 (to P.T.), NIH 10193SC (to P.T.), CA209891 (to P.T., J.S.G., and X.F.), CA102310 (to D.D.S.), T32GM007752 (to N.A.), DGE-1650112 (to N.A.), T32CA067754-22 (to A.K.), 111 Project of MOE (B14038) China (to Q.C. and X.F.), the National Natural Science Foundation (81672677, 81520108009, 81621062) China (to X.F.), the National Natural Science Foundation (81520108009 and 81621062) China (to Q.C.), and Associazione Italiana per la Ricerca sul Cancro (AIRC, IG 21322) Italy (to M.M. and D.C.R). This study was also partially funded by the NCI Intramural Research Program.

AUTHOR CONTRIBUTIONS

Conceptualization, X.F., E.R., and J.S.G.; Methodology, X.F., J.S.G., J.S.L., E.R., H.Y., and P.T.; Investigation, X.F., D.C.R., J.S.L., H.Y., N.A., Z.W., S.L., and A.K.; Formal Analysis, X.F., N.A., D.C.R., J.S.L., and H.Y.; Resources, J.S.L., J.A.P., G.M.K., E.K., Q.C., M.M., and D.D.S.; Writing – Original Draft, X.F., N.A., J.S.L., and J.S.G.; Writing – Review & Editing, X.F., N.A., E.K., D.D.S., P.T., E.R., and J.S.G.; Visualization, X.F., D.C.R., J.S.L., H.Y., and J.S.G.; Funding Acquisition, M.M., D.D.S., P.T., Q.C., X.F., E.R., and J.S.G.; Supervision, J.S.G.

DECLARATION OF INTERESTS

J.A.P. is an employee (Chief Scientific Officer) of VERASTEM, which has not influenced this study. Other authors declare no competing financial interests. J.S.G. is a consultant for Oncoceutics and Vividion Therapeutics, and has received research support from Kura Oncology and Mavupharma, all unrelated to the current study.

Received: August 17, 2018
Revised: December 3, 2018
Accepted: January 15, 2019
Published: February 14, 2019

REFERENCES

Armbruster, B.N., Li, X., Pausch, M.H., Herlitze, S., and Roth, B.L. (2007). Evolving the lock to fit the key to create a family of G protein-coupled receptors potently activated by an inert ligand. Proc. Natl. Acad. Sci. U S A *104*, 5163–5168.

Arnold, J.J., Blinder, K.J., Bressler, N.M., Bressler, S.B., Burdan, A., Haynes, L., Lim, J.I., Miller, J.W., Potter, M.J., Reaves, A., et al. (2004). Acute severe visual acuity decrease after photodynamic therapy with verteporfin: case reports from randomized clinical trials-TAP and VIP report no. 3. Am. J. Ophthalmol. *137*, 683–696.

Azab, M., Benchaboune, M., Blinder, K.J., Bressler, N.M., Bressler, S.B., Gragoudas, E.S., Fish, G.E., Hao, Y., Haynes, L., Lim, J.I., et al. (2004). Verteporfin therapy of subfoveal choroidal neovascularization in age-related macular degeneration: meta-analysis of 2-year safety results in three randomized clinical trials: treatment of age-related macular degeneration with photodynamic therapy and verteporfin in photodynamic therapy study report no. 4. Retina *24*, 1–12.

Barbazetto, I.A., Lee, T.C., Rollins, I.S., Chang, S., and Abramson, D.H. (2003). Treatment of choroidal melanoma using photodynamic therapy. Am. J. Ophthalmol. *135*, 898–899.

Barretina, J., Caponigro, G., Stransky, N., Venkatesan, K., Margolin, A.A., Kim, S., Wilson, C.J., Lehar, J., Kryukov, G.V., Sonkin, D., et al. (2012). The Cancer Cell Line Encyclopedia enables predictive modelling of anticancer drug sensitivity. Nature *483*, 603–607.

Basile, B., Marsal, J., and DeJong, T.M. (2003). Daily shoot extension growth of peach trees growing on rootstocks that reduce scion growth is related to daily dynamics of stem water potential. Tree Physiol *23*, 695–704.

Basu, A., Bodycombe, N.E., Cheah, J.H., Price, E.V., Liu, K., Schaefer, G.I., Ebright, R.Y., Stewart, M.L., Ito, D., Wang, S., et al. (2013). An interactive resource to identify cancer genetic and lineage dependencies targeted by small molecules. Cell *154*, 1151–1161.

Bhatt, M., Shah, S., and Shivprakash. (2010). Development of a high-throughput method for the determination of ethosuximide in human plasma by liquid chromatography mass spectrometry. J. Chromatogr. B Analyt Technol. Biomed. Life Sci. *878*, 1605–1610.

Cancer Genome Atlas Research Network, Weinstein, J.N., Collisson, E.A., Mills, G.B., Shaw, K.R., Ozenberger, B.A., Ellrott, K., Shmulevich, I., Sander, C., and Stuart, J.M. (2013). The cancer genome atlas pan-cancer analysis project. Nat. Genet. *45*, 1113–1120.

Carvajal, R.D., Piperno-Neumann, S., Kapiteijn, E., Chapman, P.B., Frank, S., Joshua, A.M., Piulats, J.M., Wolter, P., Cocquyt, V., Chmielowski, B., et al. (2018). Selumetinib in combination with dacarbazine in patients with metastatic uveal melanoma: a phase III, multicenter, randomized trial (SUMIT). J. Clin. Oncol. *36*, 1232–1239.

Carvajal, R.D., Sosman, J.A., Quevedo, J.F., Milhem, M.M., Joshua, A.M., Kudchadkar, R.R., Linette, G.P., Gajewski, T.F., Lutzky, J., Lawson, D.H., et al. (2014). Effect of selumetinib vs chemotherapy on progression-free survival in uveal melanoma: a randomized clinical trial. JAMA *311*, 2397–2405.

Chen, X., Wu, Q., Depeille, P., Chen, P., Thornton, S., Kalirai, H., Coupland, S.E., Roose, J.P., and Bastian, B.C. (2017). RasGRP3 mediates MAPK pathway activation in GNAQ mutant uveal melanoma. Cancer Cell *31*, 685–696.e6.

Cheung, H.W., Cowley, G.S., Weir, B.A., Boehm, J.S., Rusin, S., Scott, J.A., East, A., Ali, L.D., Lizotte, P.H., Wong, T.C., et al. (2011). Systematic investigation of genetic vulnerabilities across cancer cell lines reveals lineage-specific dependencies in ovarian cancer. Proc. Natl. Acad. Sci. U S A *108*, 12372–12377.

Chikumi, H., Fukuhara, S., and Gutkind, J.S. (2002). Regulation of G protein-linked guanine nucleotide exchange factors for Rho, PDZ-RhoGEF, and LARG by tyrosine phosphorylation: evidence of a role for focal adhesion kinase. J. Biol. Chem. *277*, 12463–12473.

Cowley, G.S., Weir, B.A., Vazquez, F., Tamayo, P., Scott, J.A., Rusin, S., East-Seletsky, A., Ali, L.D., Gerath, W.F., Pantel, S.E., et al. (2014). Parallel genome-scale loss of function screens in 216 cancer cell lines for the identification of context-specific genetic dependencies. Sci. Data *1*, 140035.

Dorsam, R.T., and Gutkind, J.S. (2007). G-protein-coupled receptors and cancer. Nat. Rev. Cancer *7*, 79–94.

Feng, X., Chen, Q., and Gutkind, J.S. (2014a). Oncotargeting G proteins: the Hippo in the room. Oncotarget *5*, 10997–10999.

Feng, X., Degese, M.S., Iglesias-Bartolome, R., Vaque, J.P., Molinolo, A.A., Rodrigues, M., Zaidi, M.R., Ksander, B.R., Merlino, G., Sodhi, A., et al. (2014b). Hippo-independent activation of YAP by the GNAQ uveal melanoma oncogene through a trio-regulated rho GTPase signaling circuitry. Cancer Cell *25*, 831–845.

Friedman, A.A., Amzallag, A., Pruteanu-Malinici, I., Baniya, S., Cooper, Z.A., Piris, A., Hargreaves, L., Igras, V., Frederick, D.T., Lawrence, D.P., et al. (2015). Landscape of targeted anti-cancer drug synergies in melanoma identifies a novel BRAF-VEGFR/PDGFR combination treatment. PLoS One *10*, e0140310.

Gao, J., Aksoy, B.A., Dogrusoz, U., Dresdner, G., Gross, B., Sumer, S.O., Sun, Y., Jacobsen, A., Sinha, R., Larsson, E., et al. (2013). Integrative analysis of complex cancer genomics and clinical profiles using the cBioPortal. Sci. Signal. *6*, pl1.

Garnett, M.J., Edelman, E.J., Heidorn, S.J., Greenman, C.D., Dastur, A., Lau, K.W., Greninger, P., Thompson, I.R., Luo, X., Soares, J., et al. (2012). Systematic identification of genomic markers of drug sensitivity in cancer cells. Nature *483*, 570–U587.

Griner, E.M., and Kazanietz, M.G. (2007). Protein kinase C and other diacylglycerol effectors in cancer. Nat. Rev. Cancer *7*, 281–294.

Gutkind, J.S., Novotny, E.A., Brann, M.R., and Robbins, K.C. (1991). Muscarinic acetylcholine receptor subtypes as agonist-dependent oncogenes. Proc. Natl. Acad. Sci. U S A *88*, 4703–4707.

Gutkind, J.S., and Robbins, K.C. (1992). Activation of transforming G protein-coupled receptors induces rapid tyrosine phosphorylation of cellular proteins, including p125FAK and the p130 v-src substrate. Biochem. Biophys. Res. Commun. *188*, 155–161.

Howe, A.K. (2011). Cross-talk between calcium and protein kinase A in the regulation of cell migration. Curr. Opin. Cell Biol. *23*, 554–561.

Hu, J.K., Du, W., Shelton, S.J., Oldham, M.C., DiPersio, C.M., and Klein, O.D. (2017). An FAK-YAP-mTOR signaling axis regulates stem cell-based tissue renewal in mice. Cell Stem Cell *21*, 91–106.e6.

Hubbard, K.B., and Hepler, J.R. (2006). Cell signalling diversity of the Gqalpha family of heterotrimeric G proteins. Cell Signal. *18*, 135–150.

Igishi, T., Fukuhara, S., Patel, V., Katz, B.Z., Yamada, K.M., and Gutkind, J.S. (1999). Divergent signaling pathways link focal adhesion kinase to mitogen-activated protein kinase cascades. Evidence for a role of paxillin in c-Jun NH(2)-terminal kinase activation. J. Biol. Chem. *274*, 30738–30746.

Ikeda, F., Terajima, H., Shimahara, Y., Kondo, T., and Yamaoka, Y. (2003). Reduction of hepatic ischemia/reperfusion-induced injury by a specific ROCK/Rho kinase inhibitor Y-27632. J. Surg. Res. *109*, 155–160.

Iorio, F., Knijnenburg, T.A., Vis, D.J., Bignell, G.R., Menden, M.P., Schubert, M., Aben, N., Goncalves, E., Barthorpe, S., Lightfoot, H., et al. (2016). A landscape of pharmacogenomic interactions in cancer. Cell *166*, 740–754.

Julius, D., and Nathans, J. (2012). Signaling by sensory receptors. Cold Spring Harb. Perspect. Biol. *4*, a005991.

Kalinec, G., Nazarali, A.J., Hermouet, S., Xu, N., and Gutkind, J.S. (1992). Mutated alpha subunit of the Gq protein induces malignant transformation in NIH 3T3 cells. Mol. Cell. Biol. *12*, 4687–4693.

Kovacs, M., Toth, J., Hetenyi, C., Malnasi-Csizmadia, A., and Sellers, J.R. (2004). Mechanism of blebbistatin inhibition of myosin II. J. Biol. Chem. *279*, 35557–35563.

Lachowski, D., Cortes, E., Robinson, B., Rice, A., Rombouts, K., and Del Rio Hernandez, A.E. (2018). FAK controls the mechanical activation of YAP, a transcriptional regulator required for durotaxis. FASEB J. *32*, 1099–1107.

Law, V., Knox, C., Djoumbou, Y., Jewison, T., Guo, A.C., Liu, Y., Maciejewski, A., Arndt, D., Wilson, M., Neveu, V., et al. (2014). DrugBank 4.0: shedding new light on drug metabolism. Nucleic Acids Res. *42*, D1091–D1097.

Lee, J.S., Das, A., Jerby-Arnon, L., Arafeh, R., Auslander, N., Davidson, M., McGarry, L., James, D., Amzallag, A., Park, S.G., et al. (2018). Harnessing synthetic lethality to predict the response to cancer treatment. Nat. Commun. *9*, 2546.

Li, P., Silvis, M.R., Honaker, Y., Lien, W.H., Arron, S.T., and Vasioukhin, V. (2016). alphaE-catenin inhibits a Src-YAP1 oncogenic module that couples tyrosine kinases and the effector of Hippo signaling pathway. Genes Dev. *30*, 798–811.

Liberzon, A., Birger, C., Thorvaldsdottir, H., Ghandi, M., Mesirov, J.P., and Tamayo, P. (2015). The molecular signatures database (MSigDB) hallmark gene set collection. Cell Syst. *1*, 417–425.

Marcotte, R., Brown, K.R., Suarez, F., Sayad, A., Karamboulas, K., Krzyzanowski, P.M., Sircoulomb, F., Medrano, M., Fedyshyn, Y., Koh, J.L., et al. (2012). Essential gene profiles in breast, pancreatic, and ovarian cancer cells. Cancer Discov. *2*, 172–189.

Marcotte, R., Sayad, A., Brown, K.R., Sanchez-Garcia, F., Reimand, J., Haider, M., Virtanen, C., Bradner, J.E., Bader, G.D., Mills, G.B., et al. (2016). Functional genomic landscape of human breast cancer drivers, vulnerabilities, and resistance. Cell *164*, 293–309.

Marinissen, M.J., Servitja, J.M., Offermanns, S., Simon, M.I., and Gutkind, J.S. (2003). Thrombin protease-activated receptor-1 signals through Gq- and G13-initiated MAPK cascades regulating c-Jun expression to induce cell transformation. J. Biol. Chem. *278*, 46814–46825.

Martin, D., Degese, M.S., Vitale-Cross, L., Iglesias-Bartolome, R., Valera, J.L.C., Wang, Z., Feng, X., Yeerna, H., Vadmal, V., Moroishi, T., et al. (2018). Assembly and activation of the Hippo signalome by FAT1 tumor suppressor. Nat. Commun. *9*, 2372.

Meng, Z., Moroishi, T., and Guan, K.L. (2016). Mechanisms of Hippo pathway regulation. Genes Dev. *30*, 1–17.

Moore, A.R., Ceraudo, E., Sher, J.J., Guan, Y., Shoushtari, A.N., Chang, M.T., Zhang, J.Q., Walczak, E.G., Kazmi, M.A., Taylor, B.S., et al. (2016). Recurrent activating mutations of G-protein-coupled receptor CYSLTR2 in uveal melanoma. Nat. Genet. *48*, 675–680.

Moroishi, T., Hansen, C.G., and Guan, K.L. (2015). The emerging roles of YAP and TAZ in cancer. Nat. Rev. Cancer *15*, 73–79.

Narumiya, S., Ishizaki, T., and Uehata, M. (2000). Use and properties of ROCK-specific inhibitor Y-27632. Methods Enzymol. *325*, 273–284.

Newton, A.C. (2010). Protein kinase C: poised to signal. Am. J. Physiol. Endocrinol. Metab. *298*, E395–E402.

O'Hayre, M., Vazquez-Prado, J., Kufareva, I., Stawiski, E.W., Handel, T.M., Seshagiri, S., and Gutkind, J.S. (2013). The emerging mutational landscape of G proteins and G-protein-coupled receptors in cancer. Nat. Rev. Cancer *13*, 412–424.

Pan, D. (2010). The hippo signaling pathway in development and cancer. Dev. Cell *19*, 491–505.

Prevarskaya, N., Skryma, R., and Shuba, Y. (2011). Calcium in tumour metastasis: new roles for known actors. Nat. Rev. Cancer *11*, 609–618.

Robertson, A.G., Shih, J., Yau, C., Gibb, E.A., Oba, J., Mungall, K.L., Hess, J.M., Uzunangelov, V., Walter, V., Danilova, L., et al. (2017). Integrative analysis identifies four molecular and clinical subsets in uveal melanoma. Cancer Cell *32*, 204–220.e15.

Rozengurt, E. (2007). Mitogenic signaling pathways induced by G protein-coupled receptors. J. Cell. Physiol. *213*, 589–602.

Sassone-Corsi, P. (2012). The cyclic AMP pathway. Cold Spring Harb. Perspect. Biol. *4*, https://doi.org/10.1101/cshperspect.a011148.

Schrage, R., Schmitz, A.L., Gaffal, E., Annala, S., Kehraus, S., Wenzel, D., Bullesbach, K.M., Bald, T., Inoue, A., Shinjo, Y., et al. (2015). The experimental power of FR900359 to study Gq-regulated biological processes. Nat. Commun. *6*, 10156.

Soucek, P., and Cihelkova, I. (2006). Photodynamic therapy with verteporfin in subfoveal amelanotic choroidal melanoma (a controlled case). Neuro Endocrinol. Lett. *27*, 145–148.

Subramanian, A., Tamayo, P., Mootha, V.K., Mukherjee, S., Ebert, B.L., Gillette, M.A., Paulovich, A., Pomeroy, S.L., Golub, T.R., Lander, E.S., et al. (2005). Gene set enrichment analysis: a knowledge-based approach for interpreting genome-wide expression profiles. Proc. Natl. Acad. Sci. U S A *102*, 15545–15550.

Sulzmaier, F.J., Jean, C., and Schlaepfer, D.D. (2014). FAK in cancer: mechanistic findings and clinical applications. Nat. Rev. Cancer *14*, 598–610.

Tancioni, I., Miller, N.L., Uryu, S., Lawson, C., Jean, C., Chen, X.L., Kleinschmidt, E.G., and Schlaepfer, D.D. (2015). FAK activity protects nucleostemin in facilitating breast cancer spheroid and tumor growth. Breast Cancer Res. *17*, 47.

Taniguchi, K., Wu, L.W., Grivennikov, S.I., de Jong, P.R., Lian, I., Yu, F.X., Wang, K., Ho, S.B., Boland, B.S., Chang, J.T., et al. (2015). A gp130-Src-

YAP module links inflammation to epithelial regeneration. Nature *519*, 57–62.

Teramoto, H., Malek, R.L., Behbahani, B., Castellone, M.D., Lee, N.H., and Gutkind, J.S. (2003). Identification of H-Ras, RhoA, Rac1 and Cdc42 responsive genes. Oncogene *22*, 2689–2697.

Therneau, T.M., and Grambsch, P.M. (2000). Modeling Survival Data: Extending the Cox Model (Springer).

Tsherniak, A., Vazquez, F., Montgomery, P.G., Weir, B.A., Kryukov, G., Cowley, G.S., Gill, S., Harrington, W.F., Pantel, S., Krill-Burger, J.M., et al. (2017). Defining a cancer dependency map. Cell *170*, 564–576.e16.

Van Raamsdonk, C.D., Bezrookove, V., Green, G., Bauer, J., Gaugler, L., O'Brien, J.M., Simpson, E.M., Barsh, G.S., and Bastian, B.C. (2009). Frequent somatic mutations of GNAQ in uveal melanoma and blue naevi. Nature *457*, 599–602.

Van Raamsdonk, C.D., Griewank, K.G., Crosby, M.B., Garrido, M.C., Vemula, S., Wiesner, T., Obenauf, A.C., Wackernagel, W., Green, G., Bouvier, N., et al. (2010). Mutations in GNA11 in uveal melanoma. N. Engl. J. Med. *363*, 2191–2199.

Vaque, J.P., Dorsam, R.T., Feng, X., Iglesias-Bartolome, R., Forsthoefel, D.J., Chen, Q., Debant, A., Seeger, M.A., Ksander, B.R., Teramoto, H., et al. (2013). A genome-wide RNAi screen reveals a Trio-regulated Rho GTPase circuitry transducing mitogenic signals initiated by G protein-coupled receptors. Mol. Cell *49*, 94–108.

Yamaguchi, K., Iglesias-Bartolome, R., Wang, Z., Callejas-Valera, J.L., Amornphimoltham, P., Molinolo, A.A., Cohen, E.E., Califano, J.A., Lippman, S.M., Luo, J., et al. (2016). A synthetic-lethality RNAi screen reveals an ERK-mTOR co-targeting pro-apoptotic switch in PIK3CA+ oral cancers. Oncotarget *7*, 10696–10709.

Yu, F.X., Luo, J., Mo, J.S., Liu, G., Kim, Y.C., Meng, Z., Zhao, L., Peyman, G., Ouyang, H., Jiang, W., et al. (2014a). Mutant Gq/11 promote uveal melanoma tumorigenesis by activating YAP. Cancer Cell *25*, 822–830.

Yu, F.X., Zhang, K., and Guan, K.L. (2014b). YAP as oncotarget in uveal melanoma. Oncoscience *1*, 480–481.

Yu, F.X., Zhao, B., and Guan, K.L. (2015). Hippo pathway in organ size control, tissue homeostasis, and cancer. Cell *163*, 811–828.

Zhao, B., Ye, X., Yu, J.D., Li, L., Li, W.Q., Li, S.M., Yu, J.J., Lin, J.D., Wang, C.Y., Chinnaiyan, A.M., et al. (2008). TEAD mediates YAP-dependent gene induction and growth control. Genes Dev. *22*, 1962–1971.

Zuidervaart, W., van Nieuwpoort, F., Stark, M., Dijkman, R., Packer, L., Borgstein, A.M., Pavey, S., van der Velden, P., Out, C., Jager, M.J., et al. (2005). Activation of the MAPK pathway is a common event in uveal melanomas although it rarely occurs through mutation of BRAF or RAS. Br J Cancer *92*, 2032–2038.

STAR★METHODS

KEY RESOURCES TABLE

REAGENT or RESOURCE	SOURCE	IDENTIFIER
Antibodies		
YAP	Cell Signaling Technology, MA	Cat# 14074; RRID: AB_2650491
pS127-YAP	Cell Signaling Technology, MA	Cat# 4911; RRID: AB_2218913
pS909-LATS1	Cell Signaling Technology, MA	Cat# 9157; RRID: AB_2133515
pT1079-LATS1	Cell Signaling Technology, MA	Cat# 8654; RRID: AB_10971635
LATS1	Cell Signaling Technology, MA	Cat# 3477; RRID: AB_2133513
p-MST1/MST2	Cell Signaling Technology, MA	Cat# 3681; RRID: AB_330269
MST1	Cell Signaling Technology, MA	Cat# 3682; RRID: AB_2144632
GAPDH(14C10)	Cell Signaling Technology, MA	Cat# 2118; RRID: AB_561053
α-Tubulin	Cell Signaling Technology, MA	Cat# 3873; RRID: AB_1904178
pY	Cell Signaling Technology, MA	Cat# 9411; RRID: AB_331228
HA-tag-HRP	Cell Signaling Technology, MA	Cat# 2999; RRID: AB_1264166
HA-tag	Cell Signaling Technology, MA	Cat# 3724; RRID: AB_1549585
myc-tag	Cell Signaling Technology, MA	Cat# 2278; RRID: AB_490778
pY397-FAK	Cell Signaling Technology, MA	Cat# 8556; RRID: AB_10891442
FAK	Cell Signaling Technology, MA	Cat# 3285; RRID: AB_2269034
cleaved PARP	Cell Signaling Technology, MA	Cat# 9541; RRID: AB_331426
p-ERK1/2	Cell Signaling Technology, MA	Cat# 4370; RRID: AB_2315112
ERK1/2	Cell Signaling Technology, MA	Cat# 4696; RRID: AB_390780
MOB1	Cell Signaling Technology, MA	Cat# 13730
pT35-MOB1	Cell Signaling Technology, MA	Cat# 8699; RRID: AB_11139998
Gαq(E-17)	Santa Cruz Biotech., CA	Cat# sc-393; RRID: AB_631536
FAK(C-20)	Santa Cruz Biotech., CA	Cat# sc-558; RRID: AB_2300502
RhoA	Cell Signaling Technology, MA	Cat# 2117; RRID: AB_10693922
TRIO(H120)	Santa Cruz Biotech., CA	Cat# sc-28564; RRID: AB_2272362
Rac1	BD Biosciences, CA	Cat# 610651; RRID: AB_397978
pY357-YAP	Abcam, MA	Cat# ab62751; RRID: AB_956486
LATS2	Bethyl Laboratories, TX	Cat# A300-479A; RRID: AB_2133375
pY26-MOB1A	Signalway Antibody, MA	Cat# 12878
flag-tag-HRP	Sigma-Aldrich, MO	Cat# A8592; RRID: AB_439702
Ki67	DAKO, CA	Cat# M724029-2
Bacterial and Virus Strains		
DH5alpha Competent E. coli	BioPioneer, CA	Cat# GACC-96
Stbl3 Competent E. coli	Thermo Fisher	Cat# C737303
Other		
siRNA-Non-targeting	Dharmacon, CO	Cat# D-001810-0X
siRNA-Gαq	Sigma-Aldrich, MO	Cat# SASI_Hs01_00231793
siRNA-FAK	Thermo Fisher, MA	Cat# s11485
siRNA-AKT1	Thermo Fisher, MA	Cat# s659
siRNA-MGLL	Thermo Fisher, MA	Cat# s22380
siRNA-MTHFD1	Thermo Fisher, MA	Cat# s9032
siRNA-CDK1	Thermo Fisher, MA	Cat# s464
siRNA-SIRT1	Thermo Fisher, MA	Cat# s223591
siRNA-PSMB5	Thermo Fisher, MA	Cat# s11354
siRNA-TRIO	Dharmacon, CO	Cat# L-005047-00-0005

(*Continued on next page*)

Continued

REAGENT or RESOURCE	SOURCE	IDENTIFIER
siRNA-RhoA	Dharmacon, CO	Cat# L-003860-00-0005
siRNA-Rac1	Dharmacon, CO	Cat# L-003560-00-0005
siRNA-LATS1	Sigma-Aldrich, MO	Cat# Hs01_00046128
siRNA-LATS2	Sigma-Aldrich, MO	Cat# Hs01_00158803
Recombinant DNA		
pCMV-myc-MST1	Addgene	Cat# 8847; RRID: Addgene_8847
pCMV2-FLAG-SAV1	Addgene	Cat# 18970; RRID: Addgene_18970
pcDNA3-HA-MOB1	Addgene	Cat# 32835; RRID: Addgene_32835
pcDNA3-HA-Y26F-MOB1	Generated in-lab	NA
pLENTi-HA-MOB1	Generated in-lab	NA
pLENTi-HA-Y26F-MOB1	Generated in-lab	NA
pGEX-HA-MOB1	Generated in-lab	NA
pGEX-HA-Y26F-MOB1	Generated in-lab	NA
pLVX-TetOne-FLAG-FAK	Generated in-lab	NA
p2xFLAG-CMV2-LATS1	Addgene	Cat# 18971
8xGTIIC-luciferase	Addgene	Cat# 34615; RRID: Addgene_34615
Chemicals, Peptides, and Recombinant Proteins		
alamarBlue™ Reagent	Grand Island, NY	Cat# DAL1100
FAK Kinase Enzyme System	Promega	Cat# V1971
YAP1 Recombinant Protein	Abnova	Cat# H00010413-P01
Glutathione Sepharose 4B	GE Healthcare	Cat# 17-0756-01
N/C Extraction Reagents	ThermoFisher	Cat# 78833
U73122	Sigma-Aldrich, MO	Cat# U6756
GF109203X	Sigma-Aldrich, MO	Cat# G2911
Clozapine N-oxide (CNO)	Sigma-Aldrich, MO	Cat# C0832
VS-4718 (PND-1186)	MedChemExpress	Cat# HY-13917
Blebbistatin	Sigma-Aldrich, MO	Cat# B0560
Y-27632	Sigma-Aldrich, MO	Cat# SCM075
Software and Algorithms		
ISLE	Lee et al., 2018	https://www.github.com/jooslee/ISLE
PhosphoSitePlus	Cell signaling technology, MA	
Oligonucleotides		
Y26F-MOB1-F (For point mutation)	Integrated DNA Technologies	CATGTTTTAAGAGTTCAAACTGATGAG ATCCTTCAGGGATATTCTTC
Y26F-MOB1-R (For point mutation)	Integrated DNA Technologies	GAAGAATATCCCTGAAGGATCTCATCA GTTTGAACTCTTAAAACATG
GAPDH-F	Integrated DNA Technologies	GAGTCAACGGATTTGGTCGT
GAPDH-R	Integrated DNA Technologies	TTGATTTTGGAGGGATCTCG
CTGF-F	Integrated DNA Technologies	GTTTGGCCCAGACCCAACTA
CTGF-R	Integrated DNA Technologies	GGCTCTGCTTCTCTAGCCTG
CYR61-F	Integrated DNA Technologies	CAGGACTGTGAAGATGCGGT
CYR61-R	Integrated DNA Technologies	GCCTGTAGAAGGGAAACGCT

CONTACT FOR REAGENT AND RESOURCE SHARING

Requests for further information or resources and reagents should be directed to and will be fulfilled by the Lead Contact, Dr. J. Silvio Gutkind (sgutkind@ucsd.edu). Plasmids used and generated in this study are subject to restrictions under a simple material transfer agreement (MTA) with UCSD.

EXPERIMENTAL MODEL AND SUBJECT DETAILS

Human Tumors Xenografts and VS-4718 *In Vivo* Treatment

All animal studies were carried out according the University of California San Diego (UCSD) Institutional Animal Care and Use Committee (IACUC)-approved protocol (S15195). Female NOD.Cg-Prkdcscid Il2rgtm1wjl/SzJ mice (commonly known as NOD scid gamma, Jackson Laboratory, Maine), 6 to 8 weeks of age and weighing 18 to 20 g, were used in the study of UM cells, housed in appropriate sterile filter-capped cages, and provided food and water ad libitum. All procedures were essentially as previously described (Feng et al., 2014b; Schrage et al., 2015; Vaque et al., 2013). Briefly, exponentially growing cultures were harvested, washed, resuspended in RPMI 1640, and 2 x 10^6 viable cells were transplanted subcutaneously into the flanks of mice. For tumor growth analysis, tumor volume was assessed as [(LW^2/2); where L and W represent the length and the width of the tumor]. The animals were monitored twice weekly for tumor development. Results of animal experiments were expressed as mean ± SEM of a total of tumors analyzed. To administer VS-4718 (Verastem Oncology; Needham, MA) to mice, 10 mg/ml VS-4718 was prepared in 0.5% carboxymethyl cellulose (CMC) (C5678, Sigma-Aldrich; St. Louis, MO) 0.1% Tween 80 (P1754, Sigma Aldrich; St. Louis, MO) in sterile water, 100 mg/kg administered via oral gavage twice daily, control group was treated with vehicle.

Cell Lines, Culture Procedures and Chemicals

HEK293 and HEK293T cells were cultured in DMEM (Sigma-Aldrich Inc., MO) containing 10% FBS (Sigma-Aldrich Inc., MO) and 1× antibiotic/antimycotic solution (Sigma-Aldrich Inc., MO). Culture conditions for UM cells (OMM1.3, OMM1.5, MEL202, Mel270 and 92.1) have been described elsewhere (Zuidervaart et al., 2005). SK-MEL-28 cells were purchased from ATCC and cultured following ATCC recommendations in EMEM containing 10% FBS. VS-4718 (PND-1186) was purchased from MedChemExpress (MCE) pre-prepared as a 10mM solution in DMSO. FR900359 (FR) was prepared in the lab of Dr. Evi Kostenis. Clozapine N-oxide (CNO), GF109203X, U73122, Blebbistatin, and Y-27632 were all purchased from Sigma-Aldrich Inc. (MO) and used at concentrations indicated in figure legends.

DNA Constructs

Plasmids pCEFL-HA, pCEFL-HA-GαqQL, pCEFL-HA-Gαq-DREADD, pCEFL-3x-Flag-Renilla-luciferase were described previously (Marinissen et al., 2003; Teramoto et al., 2003). pCEFL-myr-FAK was described previously (Chikumi et al., 2002; Igishi et al., 1999). Plasmids pCMV-myc-MST1 (Addgene #8847, originally from Joseph Avruch's lab), pCMV2-FLAG-SAV1 (Addgene #18970, originally from Marius Sudol' lab), pcDNA3-HA-MOB1 (Addgene #32835, originally from Kunliang Guan's lab), p2xFLAG-CMV2-LATS1 (Addgene #18971, originally from Marius Sudol's lab) and 8xGTIIC-luciferase (Addgene #34615, originally from Stefano Piccolo's Lab).

METHOD DETAILS

Bioinformatic Analysis (Identifying Clinically-Relevant Gαq-Specific Vulnerabilities of UM)

To identify the clinically-relevant vulnerabilities for UM, we performed an analysis that follows the main concepts of our previous work, ISLE (Lee et al., 2018) with modifications for Gαq-driven UM. We analyzed the cancer genome atlas (TCGA) (Cancer Genome Atlas Research Network et al., 2013) UM samples with skin cutaneous melanoma (SKCM) samples as control together with the large-scale functional (Cheung et al., 2011; Cowley et al., 2014; Marcotte et al., 2012, 2016) and drug response (Barretina et al., 2012; Friedman et al., 2015; Iorio et al., 2016) screens. We downloaded the gene expression, copy number alteration, and patient survival and other clinical characteristics of TCGA UM and SKCM cohort from cBioPortal (Gao et al., 2013) on Feb 1, 2017. We used 80 UM samples and 287 SKCM samples for our analysis. We obtained the data from cBioPortal as it integrates the mutation analysis from different TCGA centers to avoid center specific bias in mutation calls.

We denoted a tumor sample as $G\alpha q^+$ if any of the Gαq-family genes (*GNAQ*, *GNA11* and *CYSLTR2*) are either mutated or amplified in the given sample (amplification, if the Gistic score is greater than 0.35), and as $G\alpha q^-$ if the sample lacks *GNAQ*, *GNA11* and *CYSLTR2* genes mutation and amplification. First, we selected important genes in UM, that are (i) highly over expressed in $G\alpha q^+$ UM (n=77, excluding 3 $G\alpha q^-$ cases) with respect to control $G\alpha q^-$ SKCM TCGA samples (n=209) using Wilcoxon rank sum test ($p<0.05$). We filtered out (ii) those genes that are overexpressed in UM compared to all SKCM samples irrespective of Gαq status (Wilcoxon rank sum $p>0.05$), leading to 1,146 out of total 18,087 satisfying both conditions. We tested whether these genes show significant overlap with the genes overexpressed in $G\alpha q^+$ skin melanoma TCGA samples (n=78, mutation=16, amplification=65, overlap=13) compared to $G\alpha q^-$ SKCM samples using hypergeometric test, truncating the hypergeometric p values to 10^{-16}.

Second, we further selected the genes whose inactivation leads to better patient survival in UM, thus potential target of a therapy. We used a stratified Cox proportional hazard model to evaluate the association, while controlling for available potential confounders in the dataset including patients' sex and tumor stage (Therneau and Grambsch, 2000). The inactivation of 293 genes (out of 1,146 genes that passed the previous screen) show significant association with improved patient survival.

Third, we used gene essentiality (Cheung et al., 2011; Cowley et al., 2014; Marcotte et al., 2012, 2016) and drug response screens (Barretina et al., 2012; Friedman et al., 2015; Iorio et al., 2016) in a wide panel of cancer cell lines to identify the genes whose knockdown/inhibition specifically reduces $G\alpha q^+$ cell viability. We used the mutation and copy number data from the measurements on the cell lines in CCLE collection (Barretina et al., 2012) to determine the status of Gαq-family genes in these cell lines. We performed

Wilcoxon rank sum test between the essentiality or drug response values of the cell lines that are Gαq$^+$ *vs.* Gαq-. The essentiality or the drug inhibition identified 72 genes out of 293 genes (that passed the 2nd filter) that satisfy this condition.

Finally, we prioritized the druggable targets. We collected the druggable genome using the drug-to-target mapping curated in DrugBank database (Law et al., 2014) and the literature including (Barretina et al., 2012; Basu et al., 2013; Friedman et al., 2015; Gao et al., 2013; Garnett et al., 2012; Iorio et al., 2016). Our collection encompasses 756 targetable genes, including 273 targets of FDA-approved drugs, 10 targets of drugs under clinical trials, and 473 experimental drugs. We further removed the genes that belong to the same chromosomes to the Gαq-family genes to avoid the confounding effect of genomic linkage. This step led to the final set of 7 targets. The strength of the SL interactions (termed SL-score) of the 7 pairs was calculated as defined in (Lee et al., 2018).

Immunoblot Assay

Western blot assays were performed as described previously (Feng et al., 2014b). Western blots were developed using Immobilon Western Chemiluminescent HRP substrate (Millipore, MA) according to the manufacturer's instructions.

CRISPR-Cas9-Knockout

PTK2-sgRNA-CRISPR/Cas9-all-in-one-lentivector vector was purchased from Applied Biological Materials Inc. (Cat. K1752206). Lentivirus were prepared with HEK293T cells as the packaging cells as previously reported (Basile et al., 2004). To establish *PTK2*-knock out, cells were infected with the corresponding lentiviral supernatants for 16 hours, after which the media was changed to normal growth medium containing puromycin (Sigma-Aldrich Inc., MO) selection.

siRNAs Transfection

All cells were transfected using Lipofectamine® RNAiMAX Reagent (Thermo Fisher Scientific) according to manufacturer's instructions.

MOB1-Y26F Point Mutation

MOB1-Y26F point mutant was generated using the Quickchange Site-Directed Mutagenesis kit following manufacturer's instructions (Agilent Genomics, CA). pcDNA3-HA-MOB1 was used as the template and see the primers in the Key Resources Table.

Immunofluorescence

Cells cultured on coverslips were washed with PBS, fixed with 3.7% formaldehyde in phosphate-buffered saline (PBS) for 30 min, and permeabilized using 0.05% Triton X-100 for 10 min. Fixed cells were blocked with 3% FBS-containing PBS for 30 min, and incubated with YAP (Cell signaling technology, MI) antibody (in 3% FBS-PBS otherwise stated) for 1 hr at room temperature. The reaction was visualized with Alexa-labeled secondary antibodies (Invitrogen, CA). Samples were mounted in PBS buffer containing Hoechst 33342 (Molecular Probes, OR) for nuclear staining. Images were acquired with an Axio Imager Z1 microscope equipped with ApoTome system controlled by ZEN 2012 software (Carl Zeiss, NY).

Luciferase Assays

Cells were co-transfected with pCEFL-3x-Flag-Renilla-luciferase and 8xGTIIC-luciferase (Addgene 34615) in 6-well plates overnight to the detection of the luciferase activity, using a Dual-Glo Luciferase Assay Kit (Promega, WI) and a Microtiter plate luminometer (Dynex Tech., VA).

Immunohistochemistry

The following antibodies were used for immunohistochemistry anti-Ki67 (DAKO) and anti-YAP (CST). Unstained 5 μm paraffin sections were dewaxed in Safeclear II (Fisher Scientific, PA), hydrated through graded alcohols and distilled water, and washed three times with PBS. Antigens were retrieved using or 10 mM citrate buffer boiled in a microwave for 20 min (2 min at 100% power and 18 min at 10% power). The slides were allowed to cool down for 30 min at room temperature, rinsed twice with PBS, incubated in 3% hydrogen peroxide in PBS for 10 min to quench the endogenous peroxidase. The sections were then sequentially washed in distilled water and PBS, incubated in blocking solution (2.5% bovine serum albumin in PBS) for 30 min at room temperature. Excess solution was discarded and the primary antibodies were applied diluted in blocking solution at 4°C overnight. After washing with PBS, the slides were sequentially incubated with the biotinylated secondary antibody (1:400) (Vector Laboratories, CA) for 30 min and with the avidin-biotin complex, reconstituted according to the instruction of the manufacturer in PBS (Vector Stain Elite, ABC kit) (Vector Laboratories, CA), for 30 min at room temperature. The slides were developed in 3,3-diaminobenzidine (Sigma FASTDAB tablet) (Sigma Chemical, MO) diluted in distilled water under a microscope.

Immunoprecipitation

Cells were lysed with IP lysis buffer [10 mM Tris-Cl (pH 8.0), 150 mM NaCl, 1 mM EDTA, 0.3% CHAPS, 50 mM NaF, 1.5 mM Na_3VO4, protease inhibitor (Thermo Scientific, CO), 1 mM DTT, 1 mM PMSF], and centrifuged at 16,000 g for 5 min at 4°C. Supernatants were incubated with first antibody for 1 hr at 4°C, and protein G or protein A conjugated resin for another 1 hr. Resins were then washed 3 times with lysis buffer and boiled in SDS-loading buffer.

Cell Growth Assays

Cell growth assays were performed as described previously (Yamaguchi et al., 2016). Cells were cultured in 96-well-plate and treated with drugs for 72 hr. The manufacturer's instructions of Alamar Blue Cell Viability Reagent were followed to complete the assay.

3D Cell Culture

3-dimensional cultures were performed as described previously (Tancioni et al., 2015). Briefly, 10,000 cells were embedded in 1% methylcellulose diluted in growth media and plated onto 6-well poly-hydroxyethyl methacrylic acid (poly-HEMA)-coated plates.

Generation of GST-MOB Fusion Proteins

GST fusion proteins were prepared engineered, expressed in bacteria, and purified as previously described in (Martin et al., 2018) using standard procedures.

In vitro FAK Kinase Assay

Kinase reactions were performed as previously described in Bernard-Trifilo et al. Briefly, 1.5 μg of substrate (MOB1-GST, MOB1-Y26F-GST, GST-only control, or recombinant YAP) was resuspended in 40uL FAK Kinase buffer (20 mM HEPES pH 7.4, 10% glycerol, 10 mM $MgCl_2$, 10 mM $MnCl_2$, and 150 mM NaCl). 5 μL magnesium/ATP cocktail (75 mM $MgCl_2$, 20 mM MOPS pH 7.2, 25 mM β-glycerol phosphate, 5 mM EGTA, 1 mM sodium orthovanadate, 1 mM dithiothreitol) with or without 50 μM ATP was added to appropriate tubes, and placed in 32° water bath for 15 min. Samples were boiled in sample buffer and processed on SDS-PAGE.

Nuclear and Cytoplasm Extraction

Subcellular fractionated lysates were generated using NE-PER Nuclear and Cytoplasmic Extraction Reagents (Thermo Scientific, CO) following manufacturer instructions.

Statistical Analysis

All data analysis was performed using GraphPad Prism version 7.03 for Windows (GraphPad Software, CA). The data were analyzed by ANOVA test or t-test (* $p<0.05$, ** $p<0.01$, *** $p< 0.001$).

DATA AND SOFTWARE AVAILABILITY

RNAseq data have been deposited in GEO under ID code GEO: GSE126007.

Cancer Cell, Volume *35*

Supplemental Information

A Platform of Synthetic Lethal Gene Interaction Networks Reveals that the *GNAQ* Uveal Melanoma Oncogene Controls the Hippo Pathway through FAK

Xiaodong Feng, Nadia Arang, Damiano Cosimo Rigiracciolo, Joo Sang Lee, Huwate Yeerna, Zhiyong Wang, Simone Lubrano, Ayush Kishore, Jonathan A. Pachter, Gabriele M. König, Marcello Maggiolini, Evi Kostenis, David D. Schlaepfer, Pablo Tamayo, Qianming Chen, Eytan Ruppin, and J. Silvio Gutkind

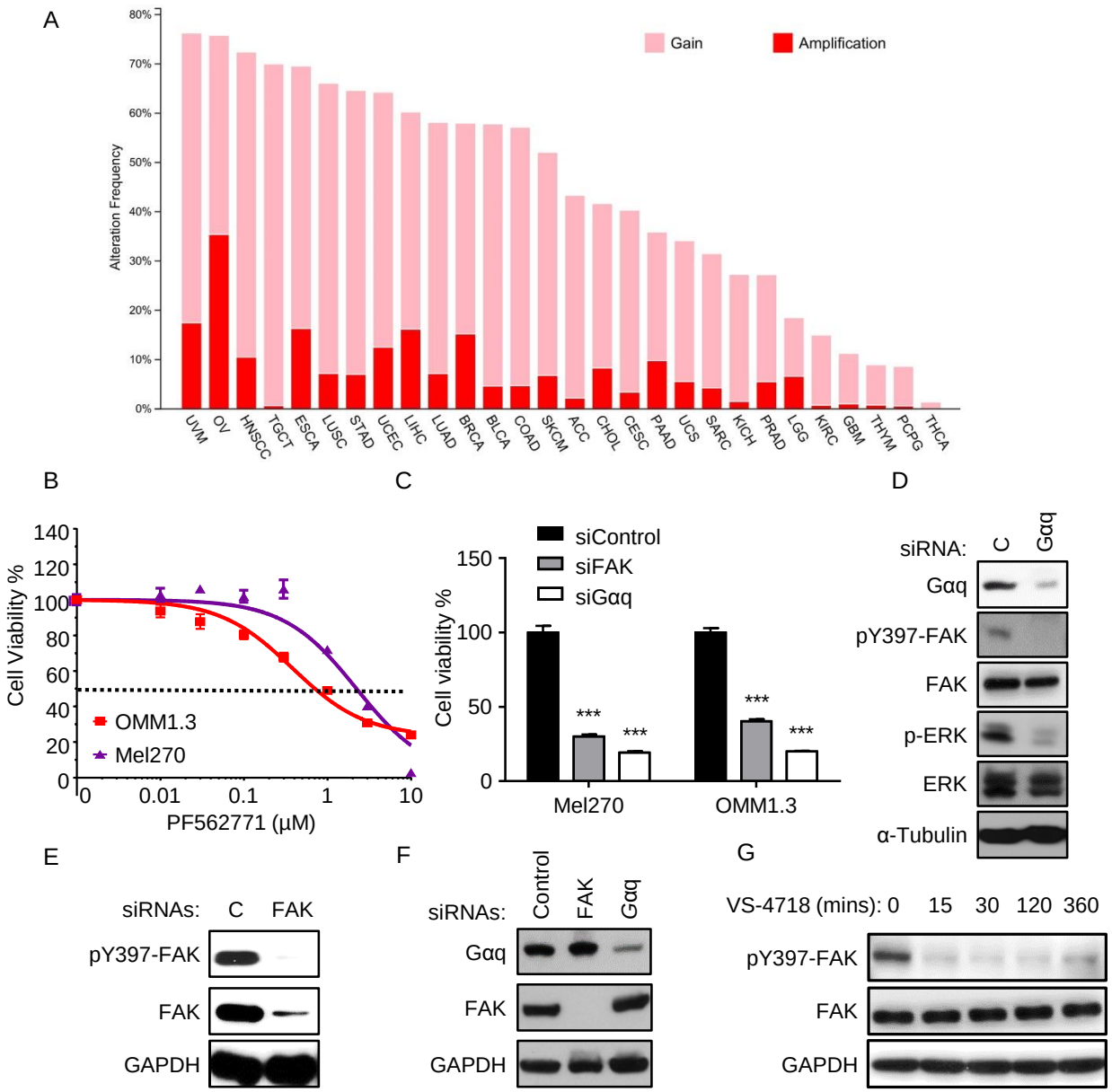

Figure S1, related to Figure 1

(A) Pan-cancer analysis of FAK alteration frequency. Data on genomic alterations (copy number gain and amplification) were downloaded from each indicated TCGA cancer cohort from cBioPortal (Gao et al., 2013). (B) Cell viability assay in UM cell lines (OMM1.3 and Mel270) after treatment with PF562771 (FAK inhibitor), percent viability is normalized to vehicle treatment (mean ± SEM, n = 3). (C) Mel270 and OMM1.3 cell viability in response to siRNA mediated FAK and Gαq knockdown (mean ± SEM, n = 3). (D) Immunoblot of siRNA mediated Gαq knockdown in OMM1.3 cells, and impact on FAK and ERK activation status. (E) Immunoblot showing total and phosphorylated FAK after siRNA mediated FAK knockdown in OMM1.3 cells. (F) Immunoblot showing levels of Gαq and FAK after siRNA mediated FAK and Gαq knockdown in Mel270 cells. (G) Immunoblot showing impact on FAK phosphorylation after a timecourse of 1μM VS-4718 treatment in Mel270 cells.

A

Oncogenic signatures gene set	Oncogenic signatures gene set (original name)	Score	0.95 MoE	p value	FDR
PDGF down-regulated genes	PDGF_UP.V1_DN	-0.864	0.184	0.001	0.200
NRL-KO up-regulated genes	NRL_DN.V1_UP	-0.863	0.173	0.002	0.200
KRAS dependency signature genes	SINGH_KRAS_DEPENDENCY_SIGNATURE_	-0.863	0.184	0.003	0.200
KRAS up-regulated genes	KRAS.300_UP.V1_UP	-0.851	0.172	0.005	0.225
Rapa up-regulated genes	MTOR_UP.N4.V1_UP	-0.818	0.164	0.008	0.270
IL21 up-regulated genes	IL21_UP.V1_UP	-0.812	0.170	0.010	0.270
YAP conserved signature genes	CORDENONSI_YAP_CONSERVED_SIGNATURE	-0.810	0.180	0.010	0.270
EGFR up-regulated genes	EGFR_UP.V1_UP	-0.800	0.179	0.012	0.270
IL15 up-regulated genes	IL15_UP.V1_UP	-0.778	0.166	0.014	0.270
PTEN-KD up-regulated genes	PTEN_DN.V2_UP	-0.775	0.175	0.014	0.270
RAD001 down-regulated genes	MTOR_UP.V1_DN	-0.736	0.183	0.019	0.318
E2F3 up-regulated genes	E2F3_UP.V1_UP	-0.721	0.158	0.023	0.336
JAK2-KD down-regulated genes	JAK2_DN.V1_DN	-0.718	0.178	0.024	0.336
BMI1-KD up-regulated genes	BMI1_DN_MEL18_DN.V1_UP	-0.716	0.168	0.025	0.336
P53-KD up-regulated genes	P53_DN.V2_UP	-0.710	0.180	0.029	0.360
BRCA1-KD up-regulated genes	BRCA1_DN.V1_DN	-0.686	0.156	0.033	0.388
Up-regulated genes in astroglia cells	CAHOY_ASTROGLIAL	-0.682	0.147	0.035	0.388
KRAS up-regulated genes	KRAS.50_UP.V1_UP	-0.659	0.164	0.043	0.440
TGFB1 down-regulated genes	TGFB_UP.V1_DN	-0.653	0.152	0.045	0.440
Late serum down-regulated genes	CSR_LATE_UP.V1_DN	-0.651	0.184	0.047	0.440

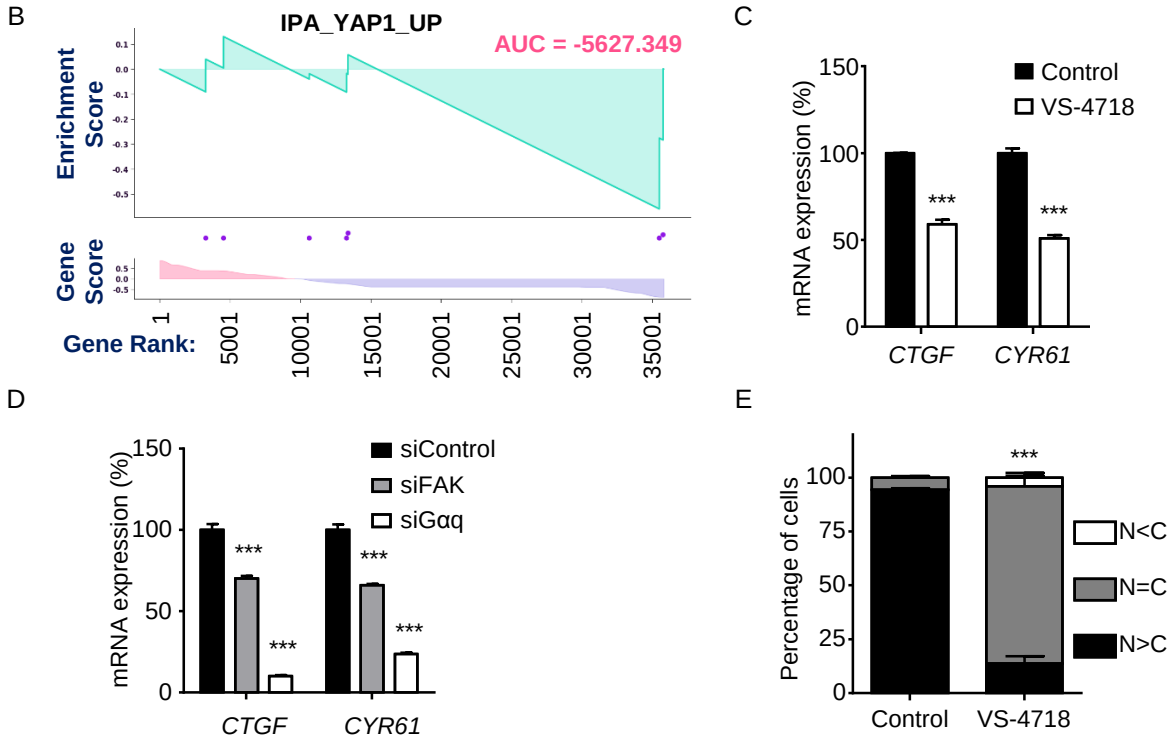

Figure S2, related to Figure 3

(A) The top 20 down-regulated oncogenic signatures gene sets from RNA-seq analysis of OMM1.3 cells treated with VS-4718 (1μM, 2 hr, vehicle treatment as control, with original gene set names). (B) Enrichment plot for IPA YAP1 upregulate gene set. (GSEA, http://software.broadinstitute.org/gsea/index.jsp). (C) mRNA expression of *CTGF* and *CYR61* measured by qPCR in Mel270 cells after 2 hr, 1 μM VS-4718 treatment (vehicle treatment as control, mean ± SEM, n = 3). (D) mRNA expression of *CTGF* and *CYR61* measured by qPCR after siRNA mediated knockdown of FAK and Gαq in Mel270 cells (mean ± SEM, n = 3). (E) Nuclear and cytoplasmic YAP quantification from Figure 3F, cytoplasm (C) and nucleus (N) (mean ± SEM, n = 3).

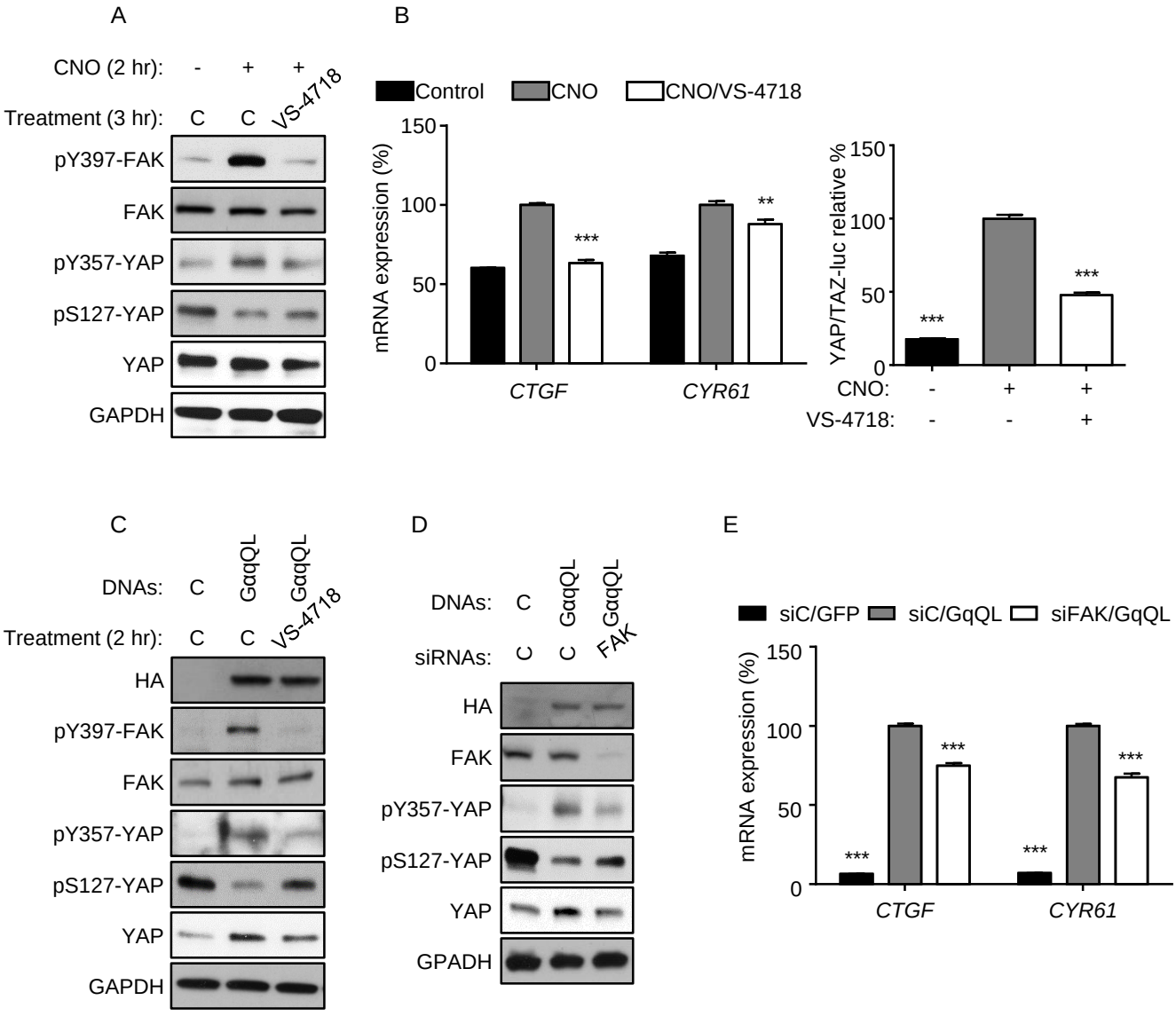

Figure S3, related to Figure 3

(A) Immunoblot showing phosphorylation of YAP after stimulation of Gαq-DREADD expressing HEK293 cells with 1μM CNO in combination with 1 μM VS-4718 treatment. (B) mRNA expression of *CTGF* and *CYR61* measured by qPCR (mean ± SEM, n = 3), and YAP/TAZ Luciferase reporter assay measuring YAP activity (mean ± SEM, n = 3) with the same treatment in the same cells as A. (C) Immunoblot showing phosphorylation of YAP after transient transfection of GαqQL and control expression vectors in HEK293 cells in combination with 1μM VS-4718 treatment. (D) Immunoblot showing phosphorylation of YAP after transient transfection of GαqQL and control expression vectors in HEK293 cells in combination with siRNA mediated FAK knockdown. (E) mRNA expression of *CTGF* and *CYR61* measured by qPCR with the same treatment in the same cells as D (mean ± SEM, n = 3).

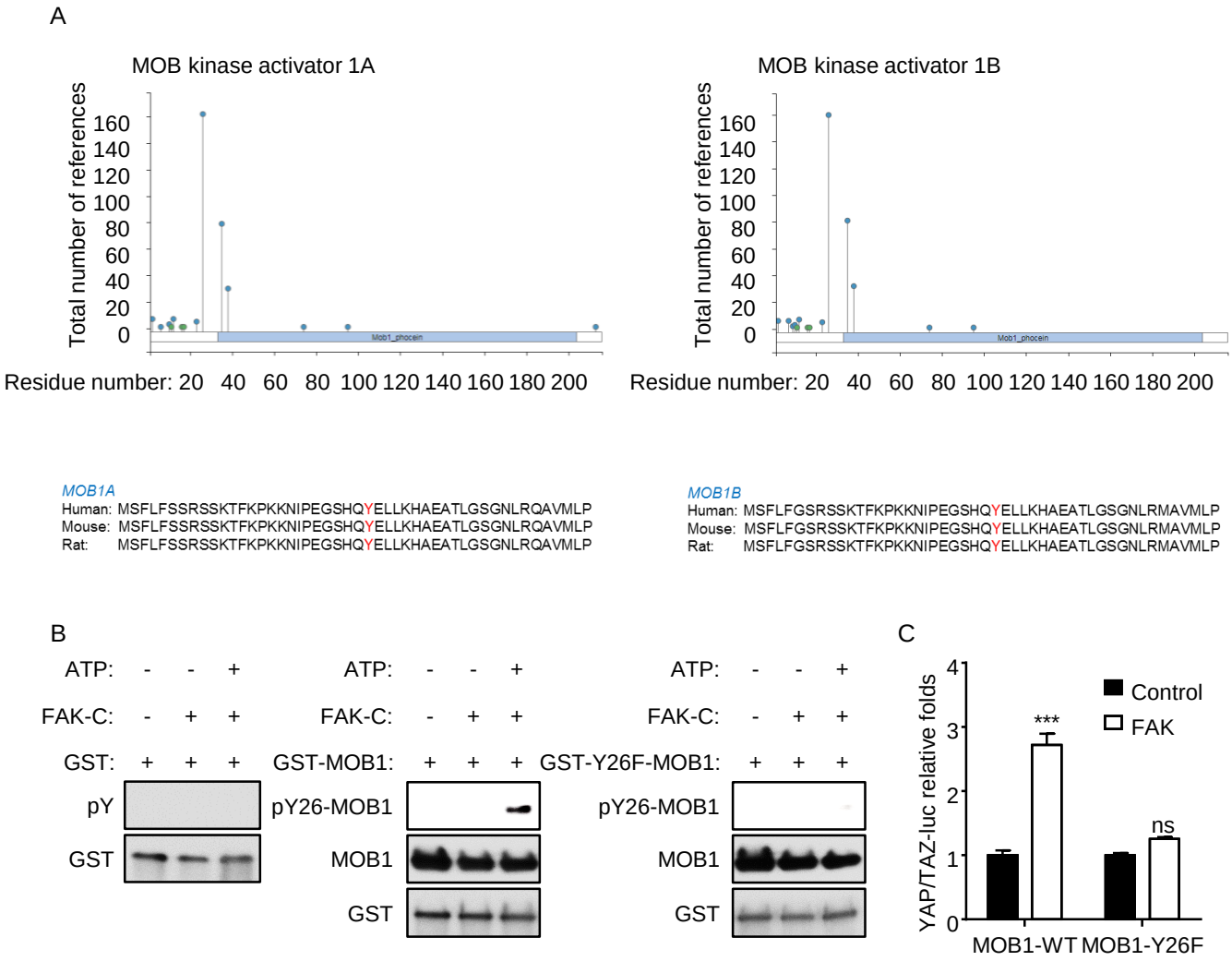

Figure S4, Related to Figure 4

(A) MOB1A and MOB1B phosphorylation sites from PhophoSitePlus (Cell Signaling Technology, https://www.phosphosite.org, top), and amino acid sequence of MOB1A and MOB1B from human, mouse and rat including tyrosine 26 (Y, red) site (bottom). (B) Y26 phosphorylation of GST-MOB1 or GST-Y26F-MOB1 (GST used as control) after *in vitro* kinase reaction using active recombinant human FAK (catalytic domain, FAK-C). (C) YAP/TAZ Luciferase reporter assay after transient transfection of HA-MOB1 or HA-MOB-Y26F, with or without FAK transfection in HEK293 cells (mean ± SEM, n = 3; ***, p<0.001, ns: not significant).

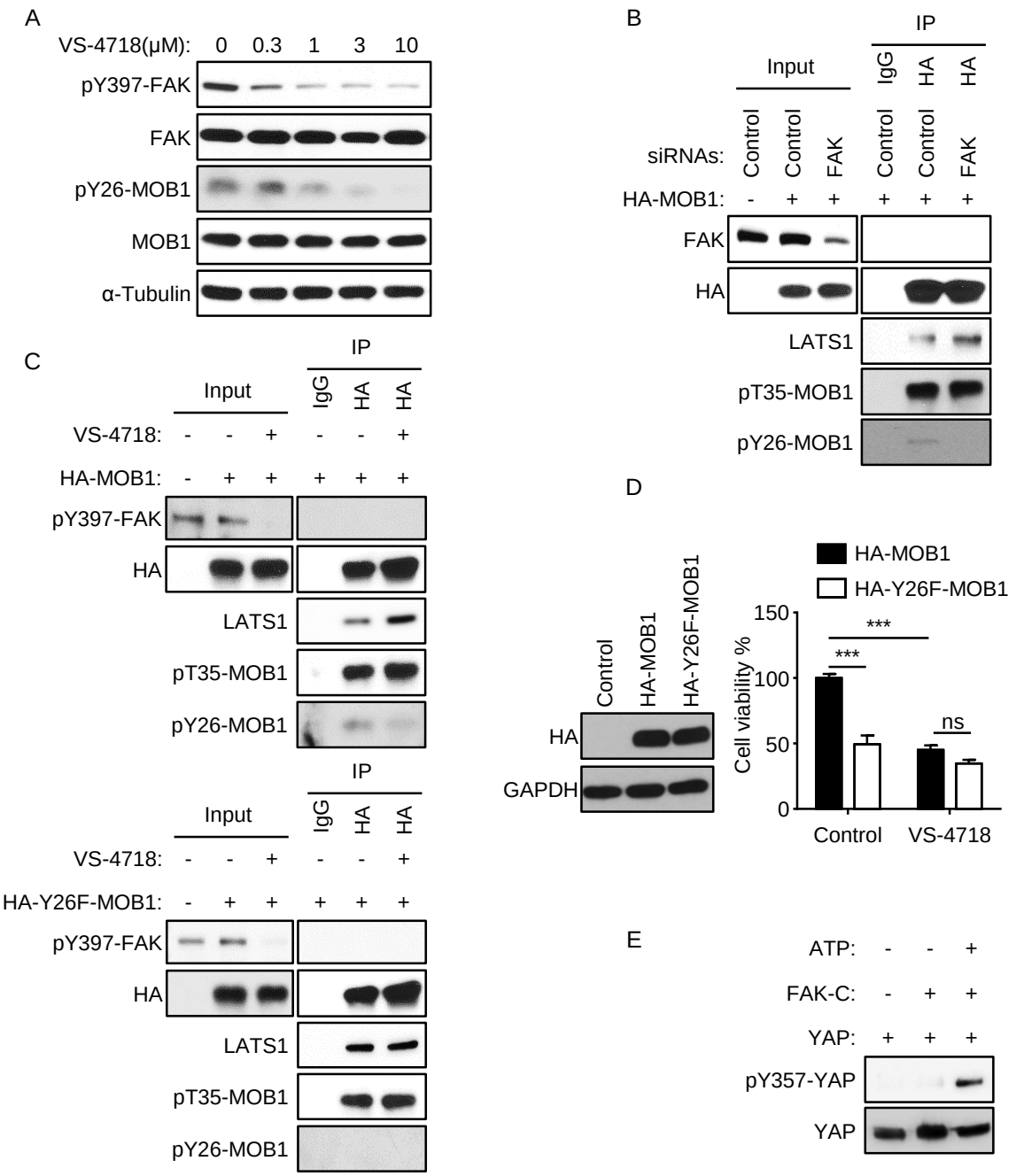

Figure S5, Related to Figure 5

(A) Immunoblot showing pY397-FAK and pY26-MOB1 with 2 hr treatment of VS-4718 at different doses in OMM1.3 cells (0-10 μM). (B) Immunoblot showing phosphorylation of HA-MOB1 and association with LATS1 after HA immunoprecipitation in OMM1.3 cells with siRNA mediated FAK knockdown. (C) Immunoblot showing phosphorylation of HA-MOB1 or HA-MOB1-Y26F and association with LATS1 after HA immunoprecipitation in OMM1.3 cells with or without VS-4718 treatment (1 μM, 2 hr). (D) Immunoblot showing HA-MOB1 and HA-Y26F-MOB1 expression in OMM1.3 (left), HA-Y26F-MOB1 expressing OMM1.3 cells phenocopy the effect of VS-4718 treatment in HA-MOB1 expressing OMM1.3 cells measured by cell viability assay (right, mean ± SEM, n = 3; ***, p<0.001; ns, not significant). (E) Immunoblot showing YAP phosphorylation after *in vitro* kinase reaction with active recombinant human FAK (catalytic domain, FAK-C).

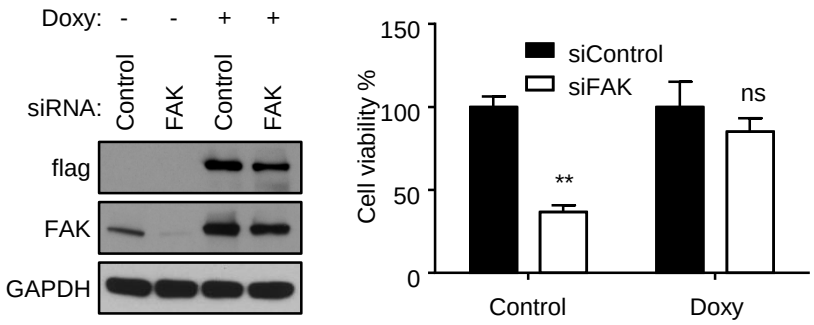

Figure S6, Related to Figure 6

Immunoblot showing siRNA mediated FAK knockdown and doxycycline-induced FAK re-expression in OMM1.3 cells (left). Impact of siRNA mediated knockdown and doxycycline-induced FAK re-expression in OMM1.3 cells as measured by cell viability assay (right, mean ± SEM, n = 3; **, p <0.01; ns, not significant).